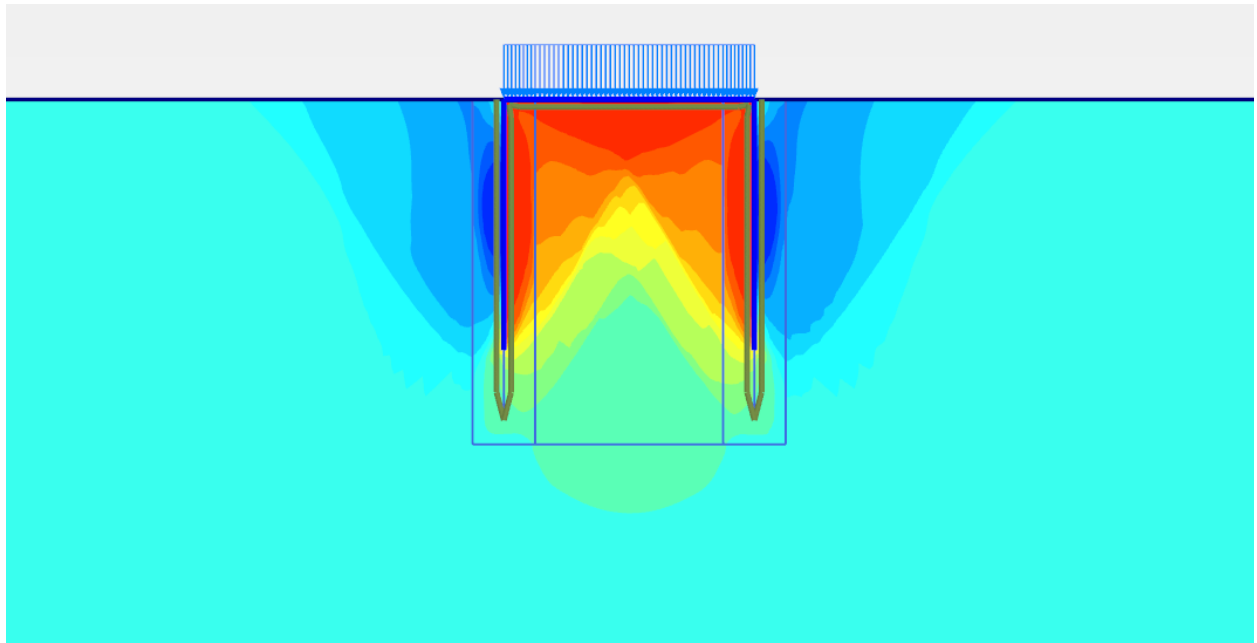# Modelling long term stability of offshore foundation under cyclic loading

Master's thesis in Infrastructure and Environmental Engineering

DAVID NYSTRÖM-PERSSON
CILING ZHOU

Modelling long term stability of offshore foundation under cyclic loading

DAVID NYSTRÖM-PERSSON
CILING ZHOU

Department of Architecture and Civil Engineering
Division of Geology and Geotechnics
CHALMERS UNIVERSITY OF TECHNOLOGY
Gothenburg, Sweden 2018

Modelling long term stability of offshore foundation under cyclic loading

DAVID NYSTRÖM-PERSSON
CILING ZHOU

Cover: Snapshot of the soil model constructed in PLAXIS 2D showing a suction caisson's displacement in Onsøy clay.

Modelling long term stability of offshore foundation under cyclic loading

DAVID NYSTRÖM-PERSSON
CILING ZHOU

Department of Architecture and Civil Engineering
Division of Geology and Geotechnics
Chalmers University of Technology

Abstract

Offshore wind turbines are increasingly more often employed in deep waters, foundation solutions in these water depths often include jacket structures with suction caissons. The long-term response of these structures will be affected by the cyclic loading, which is not explicitly taken into account in the current design methods. Additionally, the numerical modelling of these structures in general geotechnical Finite Element codes, such as PLAXIS remains unclear.

This thesis investigates the feasibility of modelling the effects of cyclic loading using an ordinary rate dependent (creep) constitutive model for soft soils and its use for simulating an axially loaded suction caisson. In the calibration stage a cyclic triaxial test is fitted at boundary value level against laboratory data on Onsøy clay using PLAXIS 2D. The experimental curve is selected as a function of the expected mean effective stress level, the loading amplitude and the loading frequency for the suction caisson studied. The calibration proved to be complicated by the Soft Soil Creep model implementation, which does not allow to fit the reference time separately.

As a result, in addition to fitting the creep rate and adapting the over consolidation ratio, a fictitious loading rate was introduced to fit the laboratory data with reasonable accuracy. Subsequent analysis of a suction caisson at boundary value level demonstrates that by introducing cyclic loading effects in the analyses. Large differences in permanent settlements and pore pressures are obtained over a 20 year life-time. Given the encountered problems in the current studies it is advised that in further studies a more comprehensive model should be used to obtain more meaningful results.

Acknowledgements

Contents

Contents

List of Figures

List of Tables

List of Tables

1
Introduction

Offshore wind turbines are often much larger than the onshore turbines due to the circumstances (Breton & Moe, 2009). The challenging environment consisting of wind, wave with varying intensity and a large overturning moment results cyclic loading and accumulated displacements in long-term in the foundation of the structure. Settlements and creep have to be studied.

Cyclic loading tends to cause volumetric reduction in the soil hence smaller capacity than a soil that is exposed to static loading, as shear strength. Because it breaks down the soil structure under loading. Considering the study is based on offshore foundation, the soil is therefore undrained; meaning no volumetric change by loading regarding the low compressibility of the water. Also, the soil capacity will be decreased by lower effective stress when the normal stress carried by the soil is transmitted to the pore water (Andersen, 2009).

There are several different types of structure design for offshore wind farms, from the monopiles to multipiles. Whereas the wind farms are being planned in deeper waters, monopiles can be less suitable. Larger overturning moment will occur and a more rigid structure will be needed. The four-legged jacket structure will be one of the solutions in order to withstand the large overturning moment. Installations methods as suctions caisson are also investigated.

The Onsøy Clay from east of Norway is evaluated in this study with sample data from wichtmann2013cyclic. Both cyclic and static tests were taken with triaxial soil test. The cyclic tests were performed in three different series and each had failure at different number of cycles. The data was used later for modelling in PLAXIS.

1.1 Aim

The aim of the study is to investigate the feasibility of modelling the effects of cyclic loading on an offshore wind turbine foundation in clay using an ordinary rate dependent (creep) constitutive model for soft soils.

1.2 Limitations

Due to time and field of competence, a few limitations had to be taken beforehand. As this is a geotechnical study, the design of the wind turbine was taken from a

baseline turbine (Jonkman, Butterfield, Musial, & Scott, 2009). Regarding the geographic location, the seismic loading will not be considered. As the study focuses on a four-legged jacket structure, overturning moment caused by a horizontal loading will be replaced with tension and compression. The Norwegian Onsøy clay is the only soil used for testing. Loading of wind and waves are simplified as a sum of each max value. All load conditions are run simultaneously during investigation. The simulation will only be programmed in PLAXIS 2D with Soft Soil Creep (SSC) and Soft Soil (SS) model.

2

Background

2.1 Literature Review

2.1.1 Offshore Wind Turbines

The installation of the first offshore wind farms were done during the 1990's with the wind turbines using available onshore technology in shallow waters, up to 20 metres depth (Arapogianni et al., 2013). It has since then been recognized that optimal offshore wind turbine design differ from the onshore design (Breton & Moe, 2009). As restrictions regarding noise are no longer a concern, larger turbines with higher efficiency for energy production can be implemented due to more reliable wind conditions existing offshore. Z. Zhang, Chen, Matveev, Nilssen, and Nysveen (2013) outline in their report that offshore application for wind energy faces circumstances that onshore technology is not equipped for. More harsh environmental conditions are to be expected and the design of components should be adapted thereafter (Arapogianni et al., 2013). It is further stated that at the beginning of the current decade, the offshore industry made technological advancements to adapt to these new conditions. Thereby increasing the 1990's average turbine rating from 0.6 MW to 3.87 MW. With current rate of development, 25 ongoing research and developement projects, new innovative solutions for the offshore wind energy industry can be expected (Arapogianni et al., 2013).

The placement of current and planned wind farms can be seen in Breton and Moe's (2009) study. They are primarily located in Europe, in shallow waters with a few test sites in deeper waters. Outlined in another study by Jonkman et al. (2009) is the importance of the wind turbine's need to be cost-effective. Closer to the shore, the wind is not as reliable as further out at sea, making the use of a large wind turbine with a high rating inefficient as the turbine does not operate at its peak. In this report the geographical situation is set to deep water conditions. Following the rationale of Jonkman et al. (2009) a wind turbine, installed in previously mentioned conditions, should have a rating of 5 MW or higher to be viable. The viability of the 5 MW rating at depths of around 50 metres is further supported by EWEA (2013) and the operational '*Beatrice*' wind farm (Beatrice Offshore Windfarm Ltd., 2017; Breton & Moe, 2009).

2.1.1.1   Substructure

There are several different substructure designs for offshore construction. The most common and widespread design is the monopile (Arapogianni et al., 2013), a steel tube with a large diameter ($<$ 7 metres) that can be seen as an extension of the wind turbine tower itself. It transfer loads through bending moment into the soil (Schaumann & Böker, 2005). Because of the simple design and relative easy installation they have been the alternative chosen for the majority of constructed wind farms. But as the technology develops and more wind farms are being planned in deeper waters, the monopile becomes less suitable as an alternative (LEANWIND Consortium, 2017). Arapogianni et al. (2013) states in their report that the technical properties of a jacket structure makes it an alternative for more deep waters, around 50 metres depth.

The jacket structure design is more suitable for supporting large wind turbines than the monopile. Due to the framework design, see figure 2.1, a more rigid structure is created to transfer loads as axial loads into the soil. According to Byrne, Houlsby, Martin, and Fish (2002) the vertical component can be expected to be low with the horizontal and overturning moment being dynamic due to harsh environmental conditions. In contrast to the monopile, the jacket structure can resist a larger overturning moment. This is because of the compression and extension of the vertical forces that occur at the base of the structure at critical loading and sets the system into a state of equilibrium.
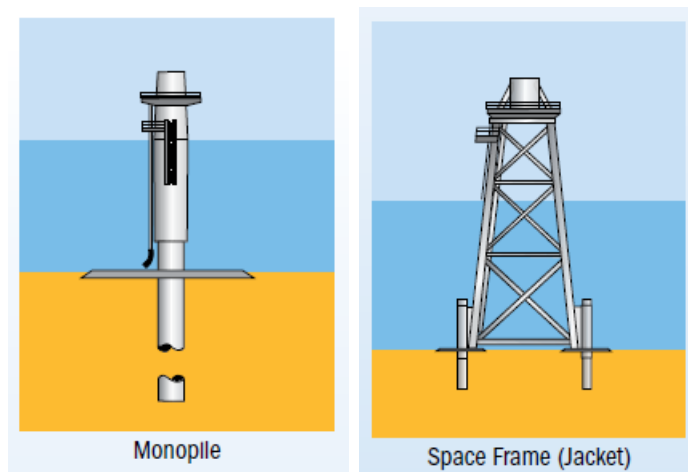
Figure 2.1: A monopile and jacket substructure design (Arapogianni et al., 2013).

2.1.1.2   Suction Caisson

A suction caisson, see figure 2.2, is a foundation design that was developed to anchor offshore gas and oil rigs to the sea floor. However, its application area extends to static structures, i.e. wind turbines, as an alternative to piles or gravity bases in deeper waters (Byrne & Houlsby, 2003; Hirai, 2017). The foundation is designed as a hollow cylinder with a top cap and can be made from either concrete or steel. The caisson is anchored to the sea floor by using its self weight to penetrate the soil.

When the mass of the caisson does not drive it any further into the soil, the trapped water inside of the caisson is pumped out. This creates a pressure differential that drives the caisson further down until full depth is reached. In the short term, the caisson remains anchored due to the pressure difference and the skin friction between the soil and the suction caisson's outside surface (Abdel-Rahman & Achmus, 2006; Andersen & Jostad, 1999). Long-term loading conditions may cause the existing under pressure inside the caisson to equalize. If this occurs, the skin friction of the caisson's inside surface will start to negate pull out of the caisson. According to Andersen and Jostad (1999) a steady state water flow will eventually be achieved in the soil and water is introduced into the caisson enabling unwanted displacements. They further state that soils of clay have more potential to resist these effects than other soils.
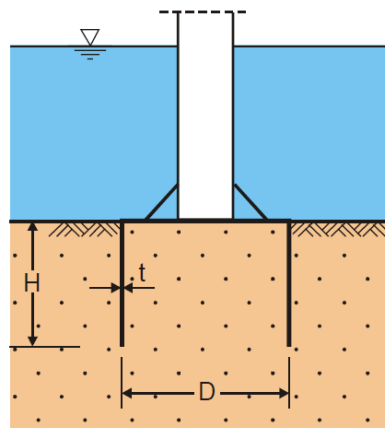
Figure 2.2: A suction caisson foundation (Abdel-Rahman & Achmus, 2006).

Spacing and footing can give different effects for a structure under loading. Calculation for separation of the footings are dependent on the structure of the footing. Typically, there are two types of existing moment; overturning moment which acts when there is a horizontal load H with a height y above the foundation and a vertical load throughout the centre of gravity of the structure. With a spacing of s for the foundation, the distance between the centre of gravity and the rotation point should be $0.5s$ for a quadratic jacket structure and $1/(2\sqrt{3})s$ for a tripod structure. In this case, the formula for the quadratic jacket structure would be considered (Byrne et al., 2002). For simplification the spacing, 25 x 25 metres, is taken from the existing jacket structure in place at the 'Beatrice' wind farm.

2.1.2 Soil

Any cemented accumulation of mineral particles formed by the weathering of rocks are defined as soil, and the void between the particles contains water or/and air. Weak cementation is due to carbonates or oxides between the particles, or due to organic matter. The particles can be transported by gravity, wind, water and

glaciers. Due to transportation, the particles can undergo change of sizes. These can be sorted into specific size ranges, varying from over 100mm to less than 0.001mm (Knappett & Craig, 2012).

2.1.2.1 Raw Data for Onsøy Clay

The study is based on the cyclic tests on high-quality undisturbed block samples of soft marine Norwegian clay. They were performed on block samples in order to compare the data with data available for standard tube samples. Three series of cyclic triaxial tests were performed by Wichtmann, Andersen, Sjursen, and Berre. According to the test results, the number of cycles to failure for a block sample was twice as high as a tube sample.

The average sensitivity of the soil is about 4.5 - 6.0 measured with a fall cone test. Furthermore, the salt content of the pore water is 32.5g/l. Most triaxial tests were performed on samples with d = 54mm and h = 108mm taken from a depth of 10.5 to 10.9 metres below the ground. The coefficient earth pressure at rest at in-situ was estimated as $K_0 = 0.6$ (Brooker & Ireland, 1965).

Sample 1 did not reach failure with more than 30 000 loading cycles applied, while the rest of the samples failed due to an accumulation of 10% permanent axial strain $\varepsilon_{a,p}$ also the permanent shear strain $\gamma_p > 15\%$.

Test series 1 was performed at the in-situ average shear stress where the samples were subjected to an undrained cyclic loading with a frequency of 0.1Hz and the average shear stress $t_{a,i}$ 0. In test series 2, the average stress was investigated at $t_{a,i} = 0$, and was carried out as an isotropic study. Lastly, test series 3 was carried out when $t_{a,i} < 0$. The large stress ratio $t_a/S_u^c > 0$ caused the failure due to accumulation of a permanent compressive strain in the first test series, while the accumulation of the extensional strain was the cause of failure in the third series.

Since the three tested series are in the range of 0 t_a/S_u^c 0.5, the undrained strength of the Onsøy clay has a plasticity index of $I_p = 33 - 34$. The sample block in the investigation has a liquid limit of $w_L = 63\%$ and plastic limit of $w_p = 29.3\%$ which gives plasticity index of 33.7%.

2.1.2.2 Anisotropy

An anisotropic material is direction dependent because of the process involved in its deposition, its composition and previous history. It can be characterized by two parts; inherent anisotropy, as a physical characteristic inherent in the material and entirely independent of the applied strains, and induced anisotropy which is entirely based on the strains that are associated with the applied stresses.

When anisotropy is possessed by a soil element in in-situ under a set of applied stresses, after being subjected to a particular stress history is a combination of both induced and inherent anisotropy and is called initial anisotropy (Zdravkovic & Potts,

2000).

Anisotropic models are rarely used because of the lack of the experimental data on soil anisotropy because of the inability of conventional laboratory equipment (Zdravkovic, Potts, & Jardine, 2001).

2.1.2.3 Isotropy

The study of soft soil begins with assuming the soil be to isotropic, and with an triaxial test in compression the undrained shear strength can be derived from the basic parameters (Zdravkovic et al., 2001).

Isotropic soils have strength parameters that are independent of the direction, for instance c, the plasticity index for cohesion, and ϕ, the friction angle. Although plane strain or shear experiments can be conducted, these parameters are usually assumed to be obtained from the triaxial tests (Zdravkovic et al., 2001).

2.1.2.4 Critical State

The critical soil mechanics describes the relation of frictional strength and consolidation by using the effective stress, σ. It includes descriptions of several behaviour factors in initial state as normally consolidated vs over-consolidated behaviour, drained vs undrained strength, cyclic behaviour, creep, strain rate, and negative vs positive pore water pressure (Tan, Phoon, Hight, & Leroueil, 2006).

With the triaxial compression mode (CIUC), the undrained shear strength can be assessed by the recommended method from (Knappett & Craig, 2012), see equation 2.1. M represents the frictional parameter in the $q - p$ space.

$$M = \frac{6 \sin \phi}{(3 - \sin \phi)} \tag{2.1}$$

2.1.3 Cyclic Loading

The properties of the soil in a given area are critical to make an accurate estimate of failure conditions. If these properties change over time, it will make accurate estimates harder to achieve and design a structure for. In an offshore environment the soil is subjected to constant cyclic loading, wave and current loads of different severity. Considering the long-term, wind load will also be taken into account under cyclic loading when the structure is in place above the sea. The general behaviour of soil subjected to cyclic loading is an induced change in its internal structure affecting its mechanical properties (Andersen, 2009; F. Zhang, Ye, Noda, Nakano, & Nakai, 2007).

Research on cyclic loading of soil agrees on that soil behaviour is highly dependent on the average and cyclic shear strain and at which frequency the load is applied (Andersen, 2009; F. Zhang et al., 2007; Andersen, Dyvik, Schrøder, Hansteen, &

Bysveen, 1993; Dyvik, Andersen, Hansen, & Christophersen, 1993). Much like in the static loading case, where shear resistance of the soil is dependent on at which rate the load is applied. A faster rate of loading gives an increased resistance to shear. Soil subjected to cyclic loading also shows a dependency on the rate of loading when evaluating shear resistance. Andersen et al. (1993) noted that in their performed tests the shear resistance decreased with an increasing load level for the load cycles and the number of cycles at a given level. This lead to failure at lower loads than for the static case with large permanent displacements of the soil. In figure 2.3 the relation between the two loading conditions can be seen. It can be concluded that the bearing capacity of the soil degrades under the influence of cyclic loading. Highlighting an important aspect of the offshore conditions that must be accounted for in structural design.
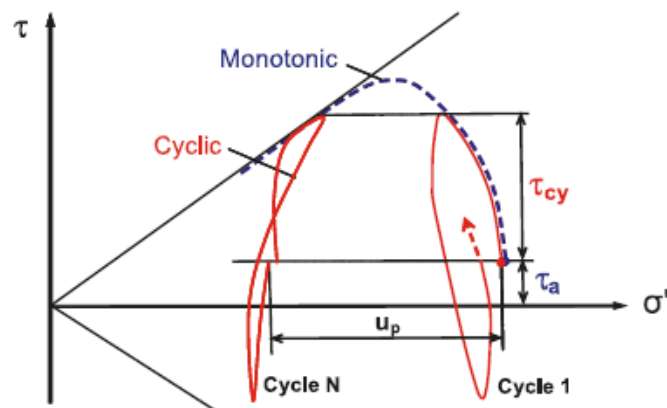
Figure 2.3: Effective stress paths of cyclic and static loading to failure (Andersen, 2009).

Andersen (2009) described in his article that an over-consolidated soil may see an increase in some properties, e.g. horizontal effective normal stress and relative density, after cyclic loading. It is further stated that the increase in the aforementioned properties may increase cyclic resistance of the soil. A fact that is substantiated by Åhnberg and Larsson (2012). They state that if soil is allowed to consolidate after cycling. The soil either regain previous properties or becomes more resistant alongside a decrease in void ratio.

For cyclic loading of soil in undrained conditions the previously mentioned structural changes are somewhat counteracted. Due to the presence of water in the soil structure, the volumetric changes implied by cyclic loading are negated by water's low compressibility, $\Delta v = 0$ (Andersen, 2009; Knappett & Craig, 2012). Instead an increase in pore pressure can be observed according to equation 2.2 which also increase with the number of loading cycles, see figure 2.4. The change in pore pressure is governed by what Wichtmann et al. (2013) noted as excess pore pressure, Δu, and the new properties are retained after the cyclic loading is stopped. In turn, the effective stress, σ , in the soil is reduced due to the new stress path as could be seen in figure 2.3.

$$u_p = u_o + \Delta u \qquad (2.2)$$
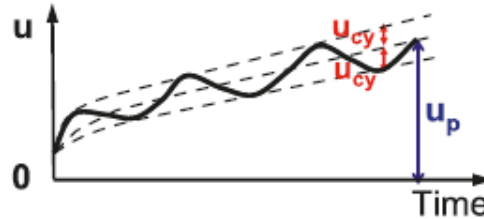
Figure 2.4: Change in pore pressure over time for a soil subjected to cycling (Andersen, 2009).

2.2 Expected Loads

The offshore development of wind turbines will be able to supply around 3.5 MW, approximately 50 times more than onshore turbines. However, it will be challenges of installing wind turbines. Comparing to onshore, the forces will be greater. The surrounding soil will be expected to stand the forces from the structure as well as the environmental loading from wind and wave (Byrne & Houlsby, 2003).

As a jacket structure is used in this study, the overturning moment will be canceled by the resisting moment from the jacket structure. The system will be in equilibrium. Hence, the maximum vertical load, F_V, and horizontal load, F_H, should also be considered. In reality, the vertical load will be relatively small compared to the overturning load. To be noted, the overturning moment represents approximately 75 % of the wind load, while only 25 % is of the horizontal load. With a period of 10 seconds per cycle and at shallow water depth approximately 10 metres, the current and wave loads will be faster than the wind loads; around 1 MN $\pm$ 2 MN.

2.3 Small Strain Stiffness

The small strain stiffness can be used for material behaviour at very small strains as $\varepsilon < 10^{-4}$. Also, it refers to when the material behaviour is linear elastic, still reversible with no plastic deformation (Wood, 2016). The small strain shear modulus is calculated with equation 2.3.

$$G_0 = \rho V_s^2 \qquad (2.3)$$

The small strain shear modulus stiffness is stress and strain magnitude dependent meaning the stiffness reduces when soil experiences shear strain. However, the soil at a lab testing will give larger stiffness than the soil in the field at small strain levels (Wood, 2016).

Figure 2.5: Reduction of shear modulus with increasing strain and ranges of strains in laboratory and field testing (Wood, 2016).

3

Method

In order to achieve the aim of the study, two material models were used to run simulations in PLAXIS 2D version 2017 to study soil response. The results of the Soft Soil Creep (S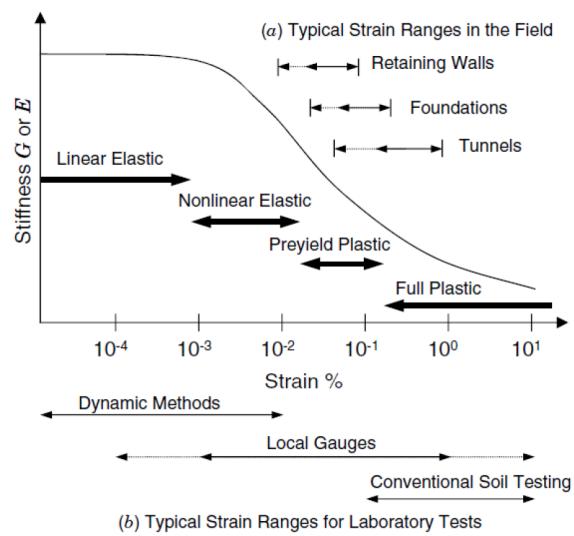SC) model and Soft Soil (SS) model were compared to each other and studied. Both were tested in an undrained condition and set up with the same value for the parameters q, p, K_0, ϕ, and M_C/M_E, derived from test data of Wichtmann et al. (2013). Swelling and compression index were calculated by the maximum shear modulus G_{max} with given parameters from Berre (2013). Apart from the previously mentioned parameters, the SSC model consists of a creep index, μ. It was defined from a triaxial soil test performed in PLAXIS 2D with data from Wichtmann et al. (2013) sample CAUC 9. Lastly, the expected loading conditions were calculated and applied to the PLAXIS model to simulate the conditions stated for the study.

3.1 Soil Properties

Soil data describing the properties of Onsøy clay is available as raw data from tests done by Wichtmann et al. (2013). It was therefore needed to distinguish the relevant information to this study from it. Which was the time until failure, the loading throughout that time period and axial strain. The available data is from static and cyclic triaxial tests, different information can be gathered from the two and will be further described in the following chapters. To view the graphs extracted from the data used in this study, see Appendix A.

3.1.1 Data Interpolation

The triaxial test result data from Wichtmann et al. (2013), the undrained test in compression (CAUC) and the undrained test in extension (CAUE) for static loads were used to interpolate input parameters, q and p, to PLAXIS 2D, see table 3.1. Equation 3.1 and 3.2 were used to calculate the parameters. p was derived by extracting the maximum value of q from a graph of q and axial strain, done for both compression and extension (Knappett & Craig, 2012).

$$q = \sigma_1 - \sigma_3 \tag{3.1}$$

$$p = \frac{\sigma_1 + 2\sigma_3}{3} \tag{3.2}$$

Based on the ratio of q and p, the slope of the critical line M, also known as the gradient of the failure envelope in tiaxial conditions, was calculated with equation 3.3.

$$\sin\phi = \frac{3M}{6+M} \tag{3.3}$$

Furthermore, the slope of the critical state line (CSL) gives the friction angle ϕ, also know as the shearing resistance. Since no cohesion is assumed, it starts from the origin. For triaxial tests with undrained shearing in compression samples CAUC-2 and CAUC-30 were calculated at their critical state. For samples CAUE-8 and CAUE-32 which are in extension, the critical state was calculated according to the same method as for compression. M is the slope of the functions in the graph as shown in figure 3.1.
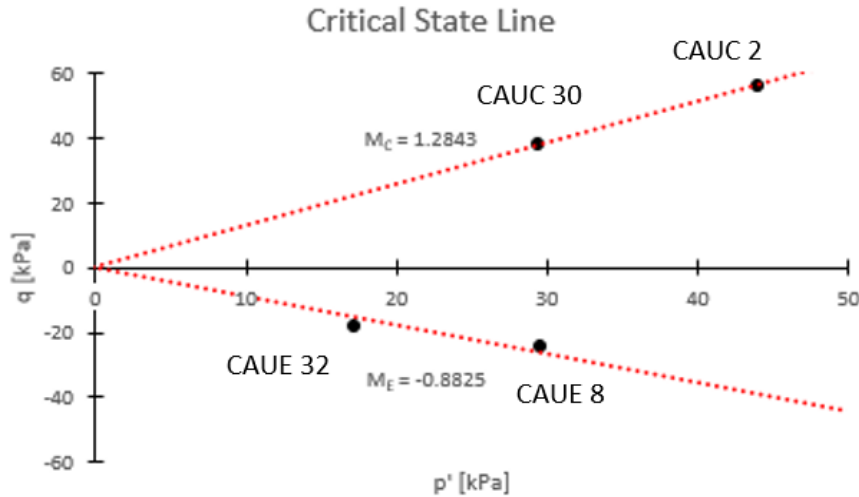
Figure 3.1: The critical state line for samples subjected to undrained shearing in compression and extension.

Table 3.1: Calculated soil properties from the static raw data of Wichtmann et al. (2013).

Sample	q [kPa]	p [kPa]	K_0 [-]	ϕ [ ]	M_C/M_E [-]
2	56.2	44.03	0.5054	31.93	1.2843
30	38.2	29.34	0.5054	31.93	1.2843
8	-20.0	25.00	-	-30.61	-0.8825
32	-16.0	15.00	-	-30.61	-0.8825

Table 3.2 shows the approximation of the modified creep index evaluated from figure 3.2 and 3.3. Note that the samples vary in value range within the same test series. This should be considered when evaluating the results as CAUC-5 differ from the

other three in the series the most. The same occurrence could be seen for CAUE-13, while the difference between CAUE-16 and CAUE-17 was large. CAUE-13 was well outside of their difference range.

The samples were plotted against the axial strain and amount of time to failure in figure 3.3. An approximation of μ is derived for each curve throughout their specified time-period before soil failure.
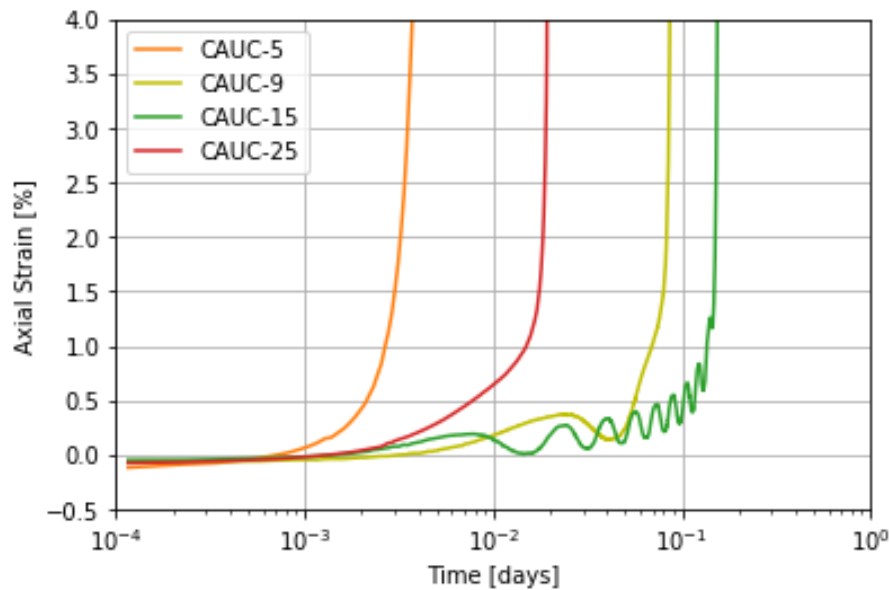
Figure 3.2: Axial strain against amount of time to failure of the samples in compression, data from Wichtmann et al. (2013).
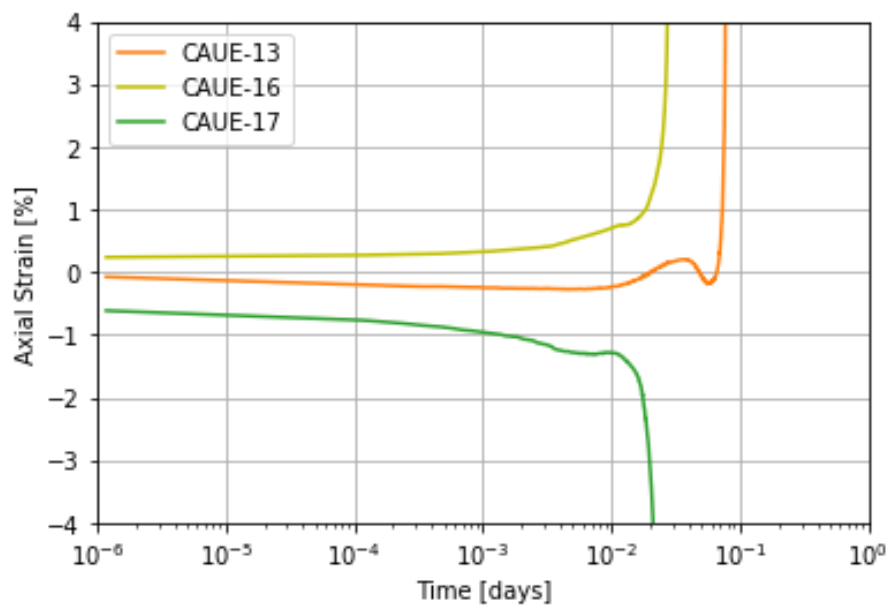
Figure 3.3: Axial strain against amount of time to failure of the samples in extension, data from Wichtmann et al. (2013).

Table 3.2: Modified creep index, μ , from the CAUC and CAUE samples of Wichtmann et al. (2013) with the average value calculated.

	CAUC-5	CAUC-9	CAUC-15	CAUC-25	**Average**
μ	0.00466	0.00322	0.00377	0.00331	**0.00374**

	CAUE-13	CAUE-16	CAUE-17		**Average**
μ	0.00530	0.0318	0.0420		**0.0264**

The maximum shear modulus G_{max} was calculated according to equation 3.4 with the parameters shown in Table 3.3. The result was used to calculate the swelling index according to equation 3.5 (Dijkstra, 2017). It is a non-linear elastic approach that is viable within the small strain area. By taking the maximum shear modulus as the reference point for the calculation. The result provided should reflect the swelling index at small strains. The parameters, e is the void ratio of the soil, v is the poisson's ratio, $v = 0.15$, and p is shown in Equation 3.2. Both e and p was set to their initial values, $e = 1.7$ and $p = 34.5$ kPa, as stated by the test results of Berre (2013) and Wichtmann et al. (2013).

$$G_{max} = \rho V_s^2 \tag{3.4}$$

Table 3.3: Shear modulus, G_{max}, of Onsøy clay (Berre, 2013).

Parameter	Unit	Onsøy clay
V_s	[m/s]	140
ρ	[kg/m^3]	1635
G_{max}	[MPa]	32.0

$$\kappa \; = \frac{3(1 - 2v\,)(1 + e)p}{2(1 + v\,)G_{max}} \tag{3.5}$$

Once the swelling index κ was known, the compression index λ was set to be near equal, but slightly higher enabling PLAXIS 2D to perform calculations. The reasoning behind this assumption was as mentioned above to investigate at small strains level and that creep alone will be used to influence a soil response of the effect of cyclic loading. Creep will therefore be controlled through the change of OCR of soil around the suction caisson's skirt wall.

3.1.2 Triaxial Test Model

The Soil Test function of PLAXIS was going to be used to establish a fit to test data of Wichtmann et al. (2013). It was however discovered that the Soil Test function operated with simplified calculation methods could not produce the desired results to fit the test data of Wichtmann et al. (2013). Therefore, a triaxial soil test was simulated in PLAXIS 2D itself. Axial strain could be evaluated throughout the test time-period without a defined axial strain increment for each time step. The data

of CAUC-9 from Wichtmann et al. (2013) was used as a baseline to set the time interval and initial effective stress, which was 40.9 kN/m^2. The triaxial test was modelled in PLAXIS 2D with the dimensions $h = 108$ mm and $d = 55$ mm.

The triaxial test simulation was first run to investigate the soil response due to the model setup and the applied soil properties. Corrections were made to the model with regard to the result of the simulation. The result had indicated an unexpected weak soil, where the K_0^{nc} value was too low compared to traditional K_0^{nc} values for clay. Due to limitations in PLAXIS 2D, in order to allow K_0^{nc} to achieve a satisfactory value of about 0.5 - 0.6, the poisson's ratio had to be changed to $v_{ur} = 0.33$ to account for the undrained condition in the test. The simulation was run again and satisfactory results for the soil properties were obtained.

To fit the triaxial soil test simulation result to CAUC-9, the creep index μ was first set to $3.74 \cdot 10^{-3}$, which was the average of the four compression samples, CAUC-5, CAUC-9, CAUC-15 and CAUC-25. To investigate the effects of OCR on the soil, a sensitivity study was performed with different OCR values by varying the pre-consolidation stress while initial stress stays the same; OCR 1.0, 1.1, 1.5 and 1.8 were tested. It was concluded that OCR did not have the desired effect on the simulation result for the created triaxial test model, see Appendix D for complete data set. During further testing of the model it was discovered that the time-period for the test had the most significant effect to be able to achieve a fit of the curve. In figure 3.4, four different time-periods are compared, where $t = 1.0$ was chosen as the best fit to the measured data for CAUC-9.
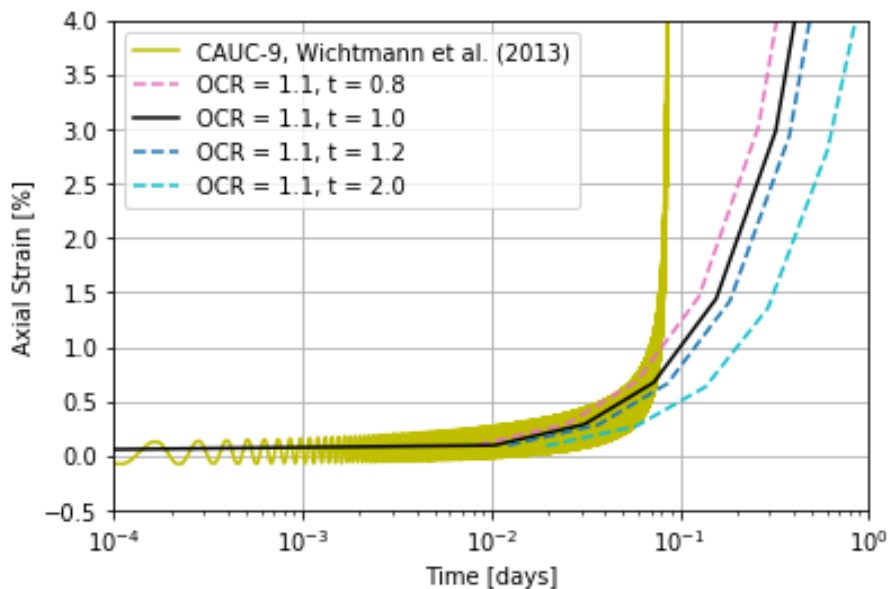

Figure 3.4: Fitting of simulated result from a triaxial test made in PLAXIS 2D to Wichtmann et al. (2013) CAUC-9 data.

The creep index μ dictated the slope of the curve, a lower creep index than $\mu = 3.74 \cdot 10^{-3}$ had no effect, while a higher value decreased the slope. The best fit

was achieved with the average value of the four compression samples. For resulting parameters and curve see table 3.4 and figure 3.5.

Table 3.4: Soil parameters used in PLAXIS 2D for SSC and SS model.

Parameter	Unit	Value	Parameter	Unit	Value
λ	[-]	0.002655	c_{ref}	[kN/m^2]	1.000
κ	[-]	0.002654	ϕ	[ ]	31.93
μ	[-]	0.003740	ψ	[ ]	0.000
v_{ur}	[-]	0.3300	TS	[MPa]	0.000
K_0^{nc}	[-]	0.4927	γ_u	[kN/m^3]	16.50
M	[-]	1.284	γ_s	[kN/m^3]	16.50
e_{init}	[-]	1.700			
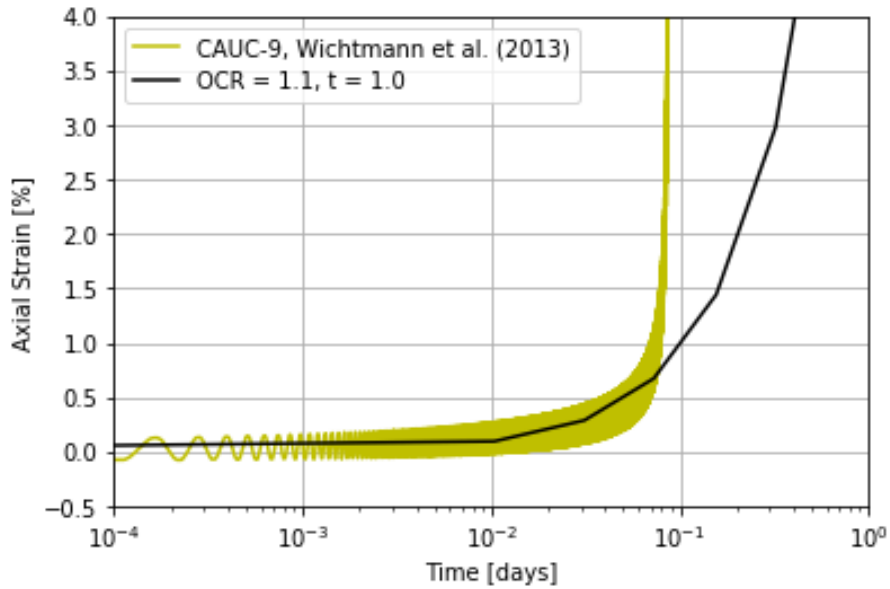
Figure 3.5: Fitting of the result from a triaxial test made in PLAXIS 2D to Wichtmann et al. (2013) sample 9 data.

3.1.3 Strain Rate

As mentioned in chapter 3.1.2, it was discovered that the time-period for the test had the most significant effect to be able to achieve a fit of the curve. According to Gras, Sivasithamparam, Karstunen, and Dijkstra (2017), 0.001 mm/min or 1.44 %/day are the requirements of loading for the drained triaxial test and 0.01 mm/min or 14.4 %/day for the undrained triaxial tests with a final axial strain of 5 %. The Wichtmann et al. (2013) tests seem to have concluded the same in the undrained triaxial soil tests in extension. In the undrained triaxial compression tests the final axial strain is up to $\varepsilon_a > 20$ % however and does not align with what Gras et al. (2017) concluded.

It is important to notice that the Wichtmann et al. tests and the triaxial test were done with different rates of strain. The former was done with a rate of 33.6 %/day until failure and the latter with 9.3 %/day for 1 day and did not fail. The rate of strain was assumed to be constant during the duration of the triaxial test. Therefore when performing PLAXIS 2D simulation, the rate of strain observed should be within the strain rate of these tests.

3.2   Cyclic Loading by Creep on a Caisson

PLAXIS 2D version 2017 was used to model the soil behaviour of Onsøy clay subjected to loading. In reality, the forces will be much larger considering, wind and wave loads. For simplification, only the vertical load is activated and tested as dynamic loading. Then evaluated using the numerical consolidation analysis of PLAXIS 2D. The setup used was a plane strain model with 15-noded elements, $y_{max} = 30$ and $x_{max} = 50$. Model setup of the suction caisson was done by plates elements with the dimension of $d = 8.0$ metres and $h = 8.0$ metres (VolkerWessels, 2018). As the focus of the study is on the behaviour of the soil, the behaviour of the steel is less interesting. Material properties of steel, see Appendix C, is therefore set to be high to avoid unwanted interference of the suction caisson in the simulation results. The soil properties used are adopted from the triaxial soil test with $\mu = 3.74 \cdot 10^{-3}$ for the SSC model as shown in table 3.4. The same parameters are used for the SS model with the exception of μ .

As mentioned above, the model settings for the soil profile was set to an area of 30 metres in height and 50 metres in width. The ground water level was set to be at +30 metres, i.e. at the seabed floor. As this is a profile located in a marine environment, the water level exceeds +30 metres in reality. To model it at a proper height above the profile will however not affect the effective stresses since it remains the same at any depth. Therefore, to minimize needless calculations in PLAXIS 2D to account for additional load, the water level was set to +30 metres.

The profile was divided into different zones with different OCR values attached, see figure 3.6, but otherwise exactly the same properties were applied. As the stiffness parameters in the material model is set to small strain conditions. The response of the soil in regards to outside influence was expected to be quite low. Also, when the compression index is close to the swelling index the stiffness of the soil will be high. This is due to the fact that conditions would remain within the failure envelope because of the small strain condition; the soil condition has to be within the elastic zone when looking into the soil behavior of creep.

In order to get an effect on the soil the inherent state parameters of the material model in the zone around the suction caisson is different from the other zones. A over consolidated soil is less compressible than the normally consolidated soil. Note that this highly over consolidated soil is bordering the deformation zone of the Onsøy clay that is created when applying loads to the model. By having OCR $= 1.1$ around the caisson allows the effects of creep to occur in the simulation within that specific

area. The soil surrounding the suction caisson's skirt walls is Onsøy clay with OCR = 1.1, whereas the soil within the suction caisson was set to be OCR = 1.5. To establish a boundary problem the outer soil was set to OCR = 3.0.
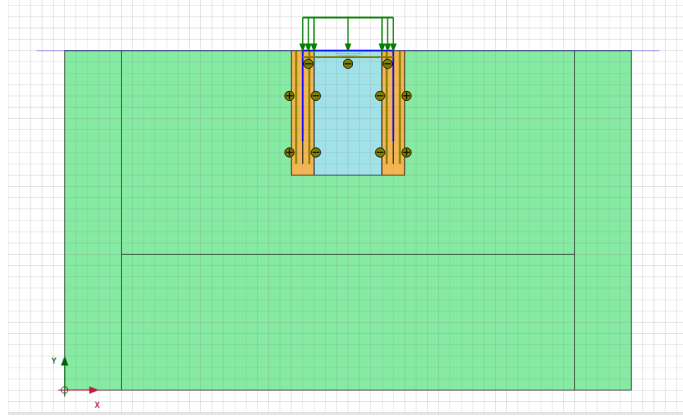

Figure 3.6: OCR = 1.1 with a SSC model in the orange zone, OCR = 1.5 with a SS model in the blue zone and OCR = 3.0 with a SS model in the green zone.

An interface was added to the plate elements to enable soil strength reduction. The reasoning for an interface is to establish more realistic aspects for the structure, where the soil in close proximity becomes remoulded. It is further used to establish the joining between the material types in PLAXIS 2D (Plaxis, 2018). To prevent a water flow through the plate element, it was set to impermeable. Making the only possible flow path available into the suction caisson be the opening at the bottom.

3.2.1 Simulation Phases

In order to calculate the soil displacement and axial strain after 7300 days, due to long term of 20 years, simulations were run in PLAXIS 2D by setting up four calculation phases, see table 3.5. K_0-procedure was chosen as the calculation type to generate the initial stresses. It allows a more manually controlled calculation of soil with a horizontal ground surface. Staged construction was chosen as the loading type for the remaining 3 phases. This was due to the step-wise introduction of new elements in the model for each phase. Add load and consolidation phases were investigated separately.

In the first phase the soil was activated and soil conditions were calculated before activating external influences. Soil zones around the structure were introduced in the initial phase with the soil parameters of the simulated triaxial test. They were set to extend 1 metre from the skirt wall on all sides. The distance was determined by running the simulation, distances shorter than 1 metre encountered failure due to mesh failure. Distances higher, was deemed to influence other aspects than the sought effect. Therefore, it was decided to use the distance of 1 metre as this ensured that calculations could be completed by PLAXIS 2D and not influence other aspects in the model more than necessary. The initial phase calculation contains a

set of initial stresses that are influenced by the weight of the material and its history of formation. At this stress state, the initial vertical effective stress and initial horizontal effective are related by the coefficient of lateral earth pressure K_0, see equation 3.6. Therefore K_0 was set to 1 for the isotropic condition.

$$\sigma_{h,0} = K_0 \cdot \sigma_{v,0} \tag{3.6}$$

The plastic calculation applies to elastic-plastic deformation while it does not consider the time in change of pore pressure. It is performed according to the small deformation theory (Plaxis, 2018).

As the following, the suction caisson with interfaces were activated in the second phase. This set the conditions for post installation and accounted for disturbance of the soil caused during the installation process through the use of interface elements. The equilibrium phase also introduces new boundaries into the simulation that will stay true throughout the rest of the simulation. Therefore, it was deemed necessary to establish these before introducing anything further. The flow paths of groundwater are recalculated as the suction caisson boundaries are impermeable.

The external loading conditions were activated in the third phase. The line load on the suction caisson lid represent the dead weight of the wind turbine and substructure. It was first tested as a dynamic load with a 0.5 day time period in 5 time steps and gradually increase towards the maximum dead weight throughout a set time-period. This was done to control the rate at which axial strain is accumulated in the soil beneath the structure before consolidation begins. Unfortunately, the strain rate was too low with a 0.5 day time period and therefore changed to 0.04 day after a intertive process of testing different time periods. Also because the affect from a dynamic loading was too small, the loading condition was then switched to apply the entire load instantly in order to accumulate a higher strain in a shorter time period. Giving a more accurate curve of ε_1 to time regarding the strain rate.

Table 3.5: Simulation phases in PLAXIS 2D.

	Phase	Calculation procedure	Pore Pressure
1	Initial	K_0-procedure	Phreatic
2	Equilibrium	Plastic, staged construction	Phreatic
3	Add Load	Plastic, staged construction	Phreatic
4	Consolidation	Consolidation, staged construction	Phreatic

Table 3.6: Load condition for line load in PLAXIS 2D model.

Parameter	Unit	Value
$q_{y,start,ref}$	[kN/m/m]	-90.23

The last phase allows all previous conditions to be active while adding a time period of 20 years. As such the suction caisson consolidated with time and an output of

soil settlements and strains can be obtained and evaluated. The consolidation phase was to calculate long-term stability of the soil when subjected loading conditions of a wind turbine. Since the average lifespan of a wind turbine can be estimated to around 20 years, the time period for consolidation was therefore set to 20 years, i.e. 7300 days in the simulation and account for small strains when calculating. By activating the small strain, calculations for insignificant deformations as creep over time can be studied (Plaxis, 2018). The results of the consolidation was recorded from the creep zone inside the suction caisson, in stress point (21.53, 23.76).

3.2.2 Model Refinement

To eliminate numerical errors in the model, a convergence study was performed. The aim was to ensure that the mesh quality of the model did not affect the calculated results. It was therefore studied by step-wise increasing the quality of the mesh in different zones and running the model through a simulation, see figure 3.7. When the results of the performed simulation converged with the previous simulation results, the mesh quality did no longer affect the results and the study was ended. The standard mesh quality used was fine with 2 times refinement in the left and right boundary zones, 4 times refinement in the top zone and 0 times refinement in the bottom zone.
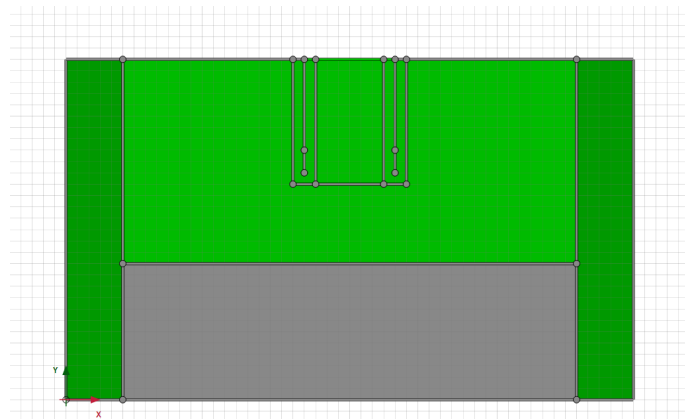

Figure 3.7: The model is divided into 6 zones with different mesh quality represented in PLAXIS 2D with shades of green.

3.2.3 Calibration of the Caisson Model

The model of the suction caisson had to have the same conditions as the soil in triaxial test before comparing the SSC and SS model. A stress point with the same initial stress as the soil in the triaxial test, 40.9 kN/m^2, was chosen to be studied. It was found at level +23.67 in the model, and was calculated with the unit weight shown above in table 3.4. Then the curve of caisson model was fitted to the triaxial test. Figure 3.8 shows the simulation result of dynamic loading in PLAXIS 2D considering creep. Through the change of OCR in PLAXIS 2D the model behaves as it is subjected to dynamic loading. The applied modified creep index was $\mu = 3.74 \cdot 10^{-3}$. The model was tested with both 0.03, 0.04 and 0.05

days. As mentioned earlier, the change of time period affects the strain rate and influences the result most. The test performed with 0.04 days is represented by the red dotted line as shown in figure 3.8. It was observed to be the best fit against the triaxial test, as it the touches two of the data points of the black line before failure. Only one of the data points were touched by the green and none by the blue line. The test result of the red curve with 0.04 days was therefore used for further investigation to compare the SSC and SS model regarding creep to each other. The same parameters was applied in both models with $\mu^* = 3.74 \cdot 10^{-3}$ as exception in the SS model.
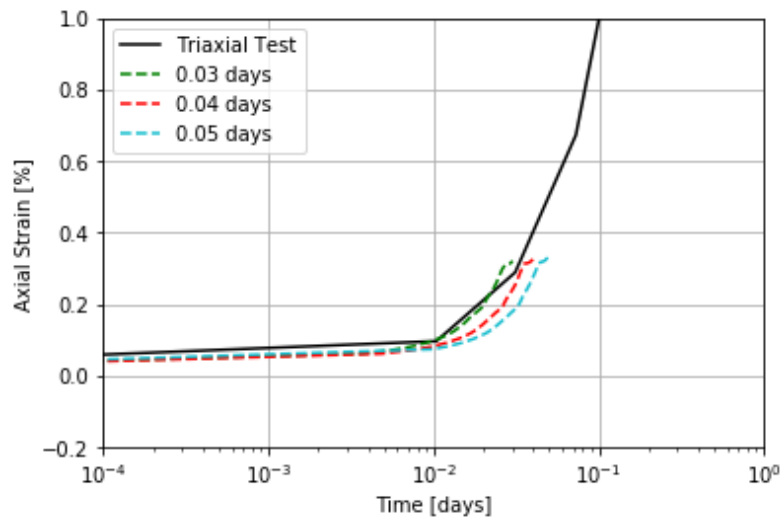

Figure 3.8: Simulation result fit of SSC model in PLAXIS 2D with triaxial test and CAUC-9 of Wichtmann et al..

4

Results

4.1 Material Model Comparison

The simulation result of axial strain development over 0.04 days for both SSC and SS is shown in figure 4.1. The SSC curve is the one from figure 3.8 in Chapter 3.2.3. With the exact same boundary conditions and parameters a SS simulation was performed and compared to the SSC model. As the detailed view of figure 4.1 clearly shows, the difference between the two simulation curves are minimum, the curve for SSC simulation is slightly higher as it might reach a failure before the SS simulation does.

Although a result that would indicate more deviation from each other might have been preferable to evaluate the real life scenario from. The similarities are somewhat expected due to the choice of where the result is being recorded. The data point is located in the creep zone at the coordinate (21.53, 23.76). These are the same coordinates that correspond to the triaxial test's initial conditions and is used as reference point. Between the triaxial test and the material model simulations, it can be deduced that the result is reasonable from the assumption that the soil should behave similar when investigated from a common standpoint.
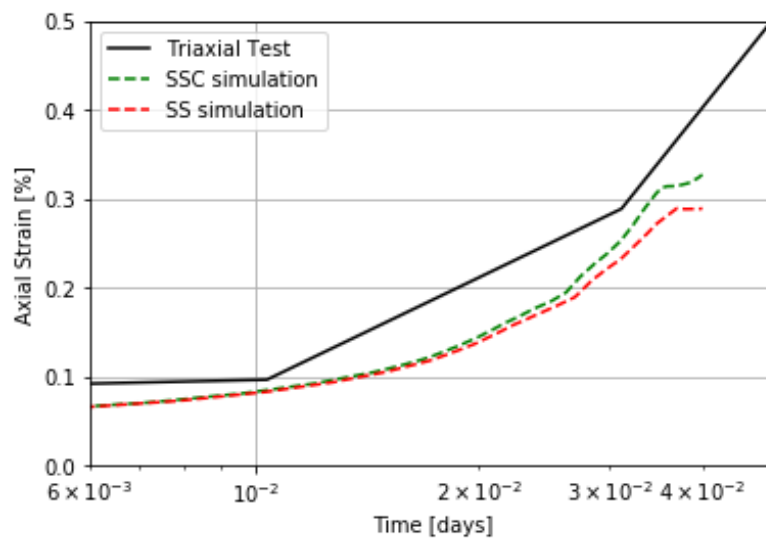

Figure 4.1: PLAXIS 2D simulation results of the SSC and SS material model.

Additional similarities between the two models can be seen in figure 4.2 and 4.3. They show the deviatoric stress distribution in the soil when the load is applied. As shown in figure 4.1 the results indicate similar behaviour between the models during this loading period. It can however be seen that the SSC simulation result have larger areas that are affected by high deviatoric stress than for the SS simulation result. The warm coloured areas presents higher deviatoric stress.
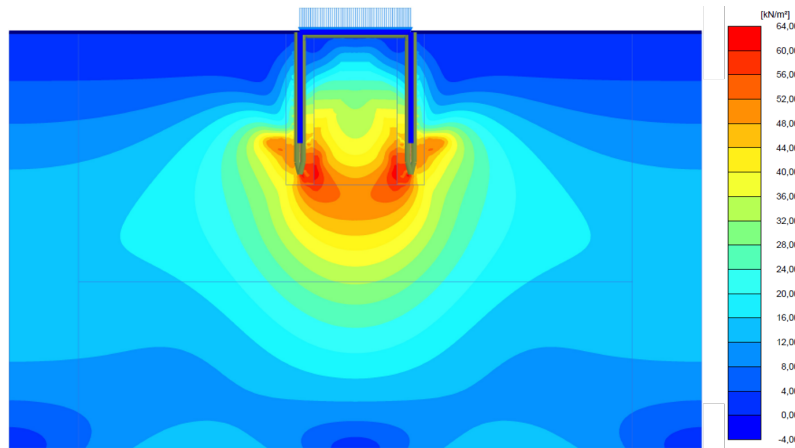

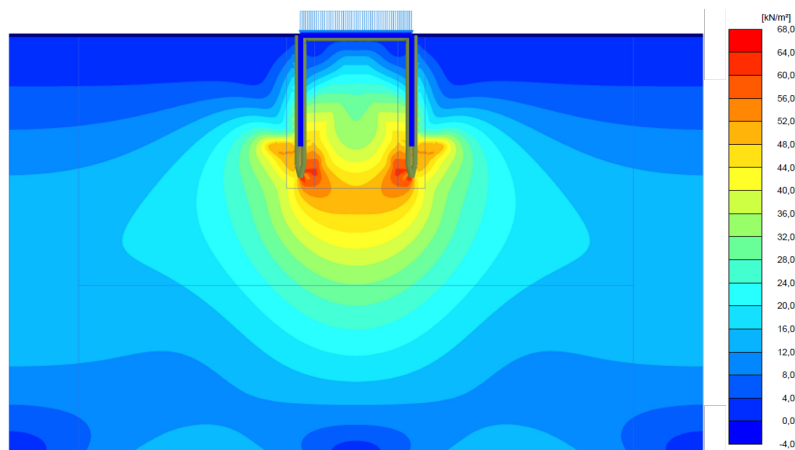**Figure 4.2:** PLAXIS 2D simulation result of deviatoric stress distribution, q, in SSC material model.

Figure 4.3: PLAXIS 2D simulation result of deviatoric stress distribution, q, in SS material model.

4.2 Consolidation of the Caisson

Figure 4.4 shows the results of the simulations performed for consolidation of the suction caisson in PLAXIS 2D. The displacement is observed from the caisson lid, node (25,30). It shows that the largest vertical displacement occurs for the SSC simulation with 112.4mm in contrast to the SS simulation with 27.7mm. This result is expected due to the effect of creep in the secondary consolidation phase that

begins when the primary consolidation phase ends. The SS simulation ends with the end of the primary consolidation phase as it does not account for creep. It can be seen that there exists a difference on how much the primary consolidation affects the total displacement. The displacement during the primary consolidation phase in the SSC simulation is in comparison to the SS simulation substantial. Suggesting that the existence of μ in the calculation affects the outcome to a large degree and that when evaluating long-term effects of consolidation note should be taken to what material model was used.
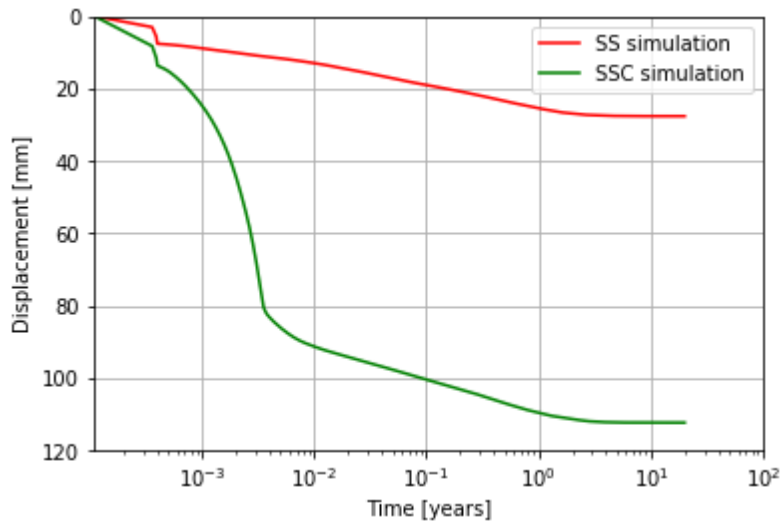

Figure 4.4: PLAXIS simulation result of the consolidation of the suction caisson over 20 years for a SS and SSC model.

The first change of inclination in the curves occurs and ends at the same time-stamp for both simulations. As this deviation occurs in both simulation it is reasonable to assume that it is not connected to the material model but the loading condition applied. A feasible assumption could be that the soil reach plastic failure due to the applied load in several nodes. The result is the rapid displacement of the caisson over a short time-period until the soil stabilizes and consolidation resume. Since the SSC simulation account for creep through the creep index, μ, a larger displacement of the soil can be observed compared to the SS simulation.

Comparing figure 4.5 to 4.6, the area affected in the SSC model is more concentrated around the caisson than the SS model. Figure 4.5 clearly shows a greater displacement under the caisson lid due to the additional creep zone, creating a weaker soil; giving a larger displacement as shown in figure 4.4. From the SSC model, one can see that the soil outside of the caisson is pushed upward because of the large downward displacement due to weaker soil. Whereas the soil is stiffer in SS model and does not behave the same way.
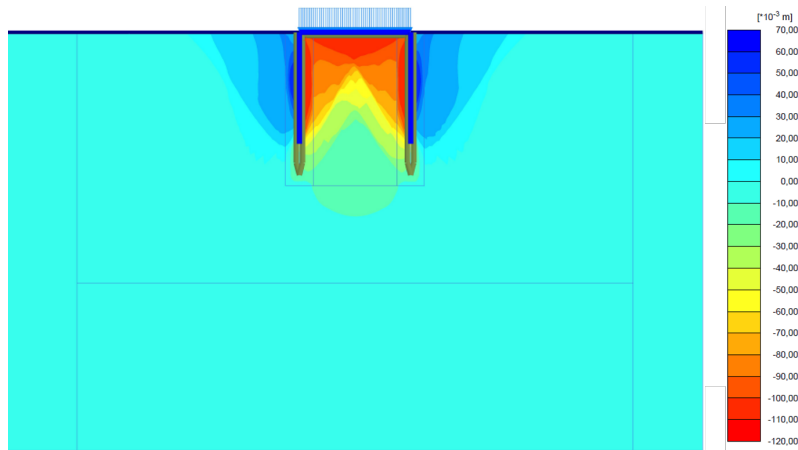
Figure 4.5: PLAXIS simulation result of the consolidation of the suction caisson over 20 years for a SSC model.
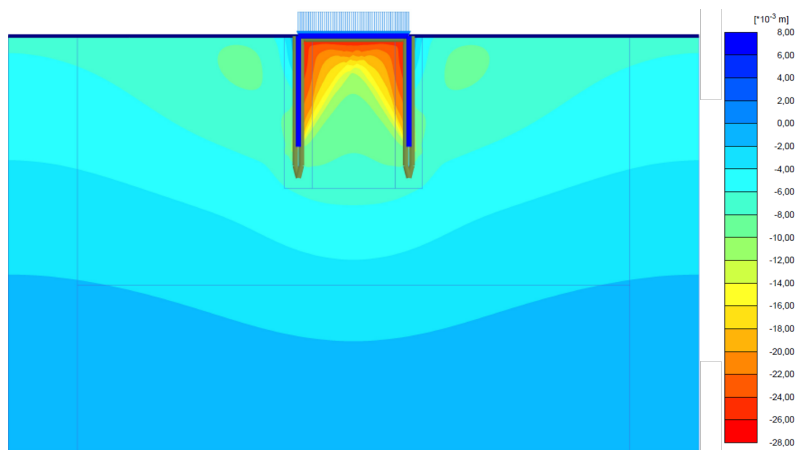

Figure 4.6: PLAXIS simulation result of the consolidation of the suction caisson over 20 years for a SS model.

Figure 4.7 shows the excess pore pressure in the reference point in relation to the displacement of the caisson lid over the consolidation period. It was expected that the excess pore pressure would begin to dissipate right after the aforementioned deviation in the curve. Instead, the p_{excess} is observed to increase until a certain point before it starts to dissipate. This behaviour is likely due to the creep of cyclic loading and appears to be an Mandel-Cryer effect delaying the consolidation. But to substantiate that theory, further tests would have to be done.

Whereas the SSC simulation is observed to have a delayed consolidation, the SS simulation shows a more expected consolidation behaviour, see figure 4.8. As the p_{excess} starts to dissipate with the displacement of the caisson, the consolidation begins directly.
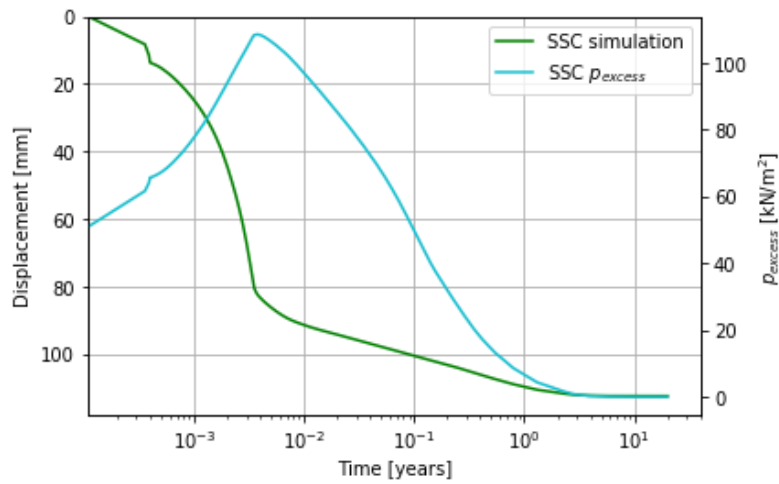
Figure 4.7: PLAXIS 2D simulation result of p_{excess} distribution throughout consolidation for SSC model.
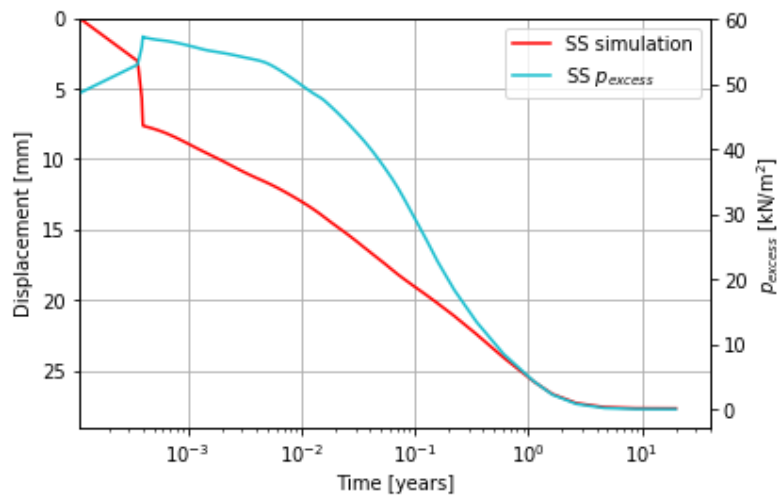
Figure 4.8: PLAXIS 2D simulation result of p_{excess} distribution throughout consolidation for SS model.

Although the start of consolidation is delayed for the SSC simulation, it levels out earlier than the SS simulation. The change in displacement thereafter can be attributed to creep, and the two should not be the same. The displacement rate for the SSC simulation is $\dot{u}_{ssc} = 8.27 \cdot 10^{-3}$ mm/year and for the SS simulation it is $\dot{u}_{ss} = 8.88 \cdot 10^{-4}$ mm/year.

5
Conclusion and Recommendations

The cyclic response of an offshore wind turbine foundation using suction caisson was investigated using a novel calibration of a rate dependent model for soft soils, i.e. Soft Soil Creep, on undrained cyclic triaxial data. The calibration procedure proved to be cumbersome as in addition to locating experimental data that is relevant for the foundation loads studies and the non-intuitive relation between the model parameters and the experimental data. A further complication was that the constitutive model used is not originally formulated for this purpose, the reference time in the creep formulation could not be altered.

As a result a best fit of the experimental data was obtained by modifying the loading rate in addition to the creep rate and the Over Consolidation Ratio (OCR). After obtaining an agreeable calibration of the model on the laboratory data the effects of incorporation of cyclic loading for an axially suction caisson was studied. Large differences in the settlements and the generation and dissipation of excess pore pressures are obtained when the 'cyclic' and static (without enabling cyclic creep) results are compared. The latter shows, although using a rudimentary calculation, that cyclic loading might affect the response of an offshore wind turbine foundation. Given the encountered difficulties using the Soft Soil Creep model it is advised that in further studies a more comprehensive model will be used to obtain more meaningful results. Finally, more experimental data on the response of soft soils under cyclic loading needs to be gathered.

References

4C Offshore. (2018). *Beatrice o shore wind farm.* Retrieved from `http://www.4coffshore.com/windfarms/beatrice-united-kingdom-uk53.html`

Abdel-Rahman, K., & Achmus, M. (2006). Behaviour of monopile and suction bucket foundation systems for offshore wind energy plants. In *5th international engineering conference, sharm el-sheikh, egypt* (Vol. 12, pp. 317–321).

Andersen, K. H. (2009). Bearing capacity under cyclic loading—offshore, along the coast, and on land. the 21st bjerrum lecture presented in oslo, 23 november 2007. *Canadian Geotechnical Journal*, *46*(5), 513–535.

Andersen, K. H., Dyvik, R., Schrøder, K., Hansteen, O. E., & Bysveen, S. (1993). Field tests of anchors in clay. ii: Predictions and interpretation. *Journal of Geotechnical Engineering*, *119*(10), 1532–1549.

Andersen, K. H., & Jostad, H. P. (1999). Foundation design of skirted foundations and anchors in clay. In *O shore technology conference.*

Arapogianni, A., Genachte, A., Ochagavia, R. M., Vergara, J., Castell, D., Tsouroukdissian, A. R., . . . others (2013). Deep water; the next step for offshore wind energy. *European Wind Energy Association (EWEA), Brussels, Belgium, ISBN*, 978–2.

Beatrice Offshore Windfarm Ltd. (2017). *Technology.* Retrieved from `https://www.beatricewind.com/technology`

Berre, T. (2013). Test fill on soft plastic marine clay at onsøy, norway. *Canadian Geotechnical Journal*, *51*(1), 30–50.

Breton, S.-P., & Moe, G. (2009). Status, plans and technologies for offshore wind turbines in europe and north america. *Renewable Energy*, *34*(3), 646–654.

Brooker, E. W., & Ireland, H. O. (1965). Earth pressures at rest related to stress history. *Canadian geotechnical journal*, *2*(1), 1–15.

Byrne, B. (2011). *Foundation design for o shore wind turbines.* Retrieved from `http://www.eng.ox.ac.uk/civil/pdf/Geotechnique_Lecture_BWB_2011_Web.pdf`

Byrne, B., & Houlsby, G. (2003). Foundations for offshore wind turbines. *Philosophical Transactions of the Royal Society of London A: Mathematical, Physical and Engineering Sciences*, *361*(1813), 2909–2930.

Byrne, B., Houlsby, G., Martin, C., & Fish, P. (2002). Suction caisson foundations for offshore wind turbines. *Wind Engineering*, *26*(3), 145–155.

Dijkstra, J. (2017). *Soil behaviour in shear.* University Lecture.

Dyvik, R., Andersen, K. H., Hansen, S. B., & Christophersen, H. P. (1993). Field tests of anchors in clay. i: Description. *Journal of Geotechnical Engineering*, *119*(10), 1515–1531.

Gras, J.-P., Sivasithamparam, N., Karstunen, M., & Dijkstra, J. (2017). Strategy for consistent model parameter calibration for soft soils using multi-objective optimisation. *Computers and Geotechnics*, *90*, 164–175.

Hirai, H. (2017). Assessment of cyclic response to suction caisson in clay using a three-dimensional displacement approach. *Marine Georesources & Geotechnology*, 1–13.

Jonkman, J., Butterfield, S., Musial, W., & Scott, G. (2009). *Definition of a 5-mw reference wind turbine for o shore system development* (Tech. Rep.). National Renewable Energy Lab.(NREL), Golden, CO (United States).

Knappett, J. A., & Craig, R. F. (2012). *Craig's soil mechanics* (8th ed.). Abingdon: Spon Press.

LEANWIND Consortium. (2017). *Driving cost reductions in o shore wind.* Retrieved from `https://windeurope.org/about-wind/reports/`

Plaxis. (2018). *Plaxis 2d reference manual 2018.* Retrieved from `https://www.plaxis.com/support/manuals/plaxis-2d-manuals/`

Schaumann, P., & Böker, C. (2005). Can jackets and tripods compete with monopiles. *Proc. Copenhagen O shore Wind*, *5*.

Tan, T. S., Phoon, K.-K., Hight, D., & Leroueil, S. (2006). *Characterisation and engineering properties of natural soils, two volume set: Proceedings of the second international workshop on characterisation and engineering properties of natural soils, singapore, 29 november-1 december 2006* (Vol. 3). CRC Press.

VolkerWessels. (2018). *Dong borkum ri grund demostrator suction bucket jacket.* Retrieved from `https://en.volkerwessels.com/en/projects/detail/dong-borkum-riffgrund-demostrator-suction-bucket-jacket`

Wichtmann, T., Andersen, K., Sjursen, M., & Berre, T. (2013). Cyclic tests on high-quality undisturbed block samples of soft marine norwegian clay. *Canadian Geotechnical Journal*, *50*(4), 400–412.

Wood, T. (2016). *On the small strain sti ness of some scandinavian clays and impact on deep excavation.* Chalmers University of Technology.

Zdravkovic, L., & Potts, D. (2000). Advances in modelling soil anisotropy. In *Constitutive modelling of granular materials* (pp. 491–521). Springer.

Zdravkovic, L., Potts, D., & Jardine, R. (2001). A parametric study of the pull-out capacity of bucket foundations in soft clay. *Géotechnique*, *51*(1), 55–67.

Zhang, F., Ye, B., Noda, T., Nakano, M., & Nakai, K. (2007). Explanation of cyclic mobility of soils: Approach by stress-induced anisotropy. *Soils and Foundations*, *47*(4), 635–648.

Zhang, Z., Chen, A., Matveev, A., Nilssen, R., & Nysveen, A. (2013). High-power generators for offshore wind turbines. *Energy Procedia*, *35*, 52–61.

Åhnberg, H., & Larsson, R. (2012). Strength degradation of clay due to cyclic loadings and enforced deformation. *Swedish Geotechnical Institute, Report*, *75*.

A
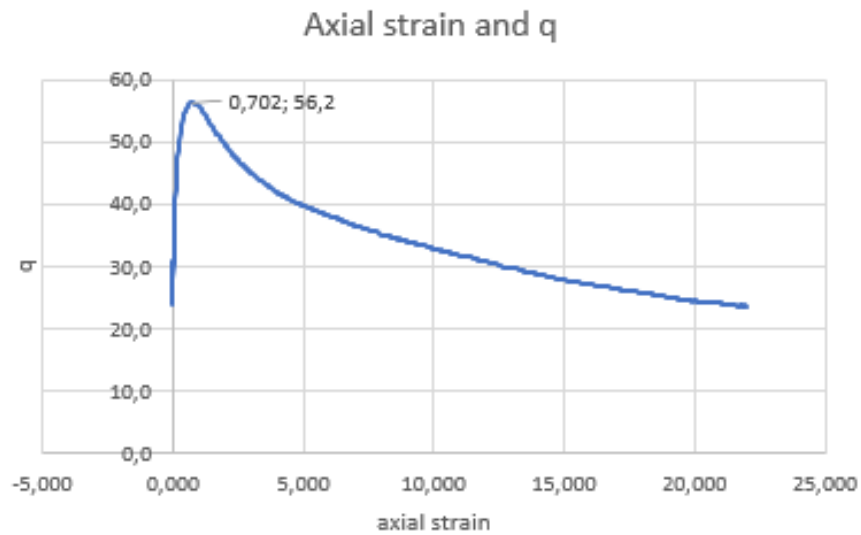## Appendix A

Graphs of CAUC and CAUE

A.1   CAUC

Axial strain and q

Figure A.1: A graph showing the axial strain, ε_a, to q for static sample 2.

Undrained axial test
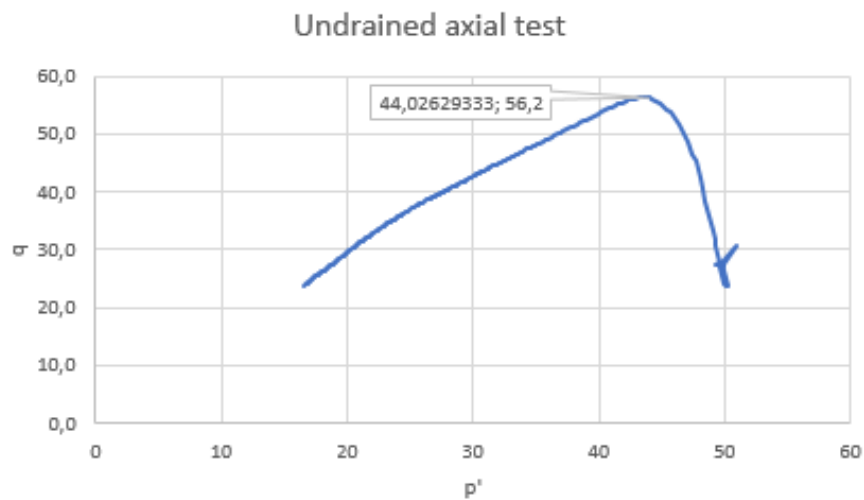
Figure A.2: A graph showing p to q for static sample 2.

II
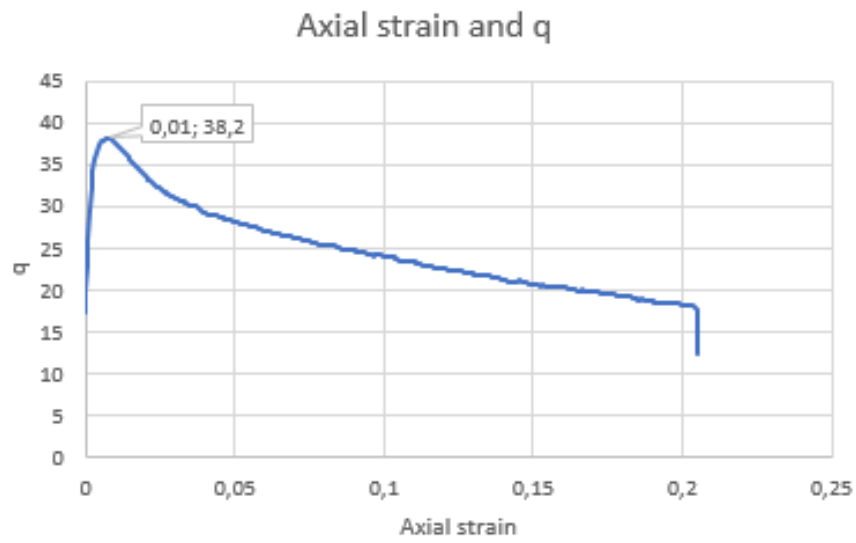
Figure A.3: A graph showing the axial strain, ε_a, to q for static sample 30.

Figure A.4: A graph showing p to q for static sample 30.
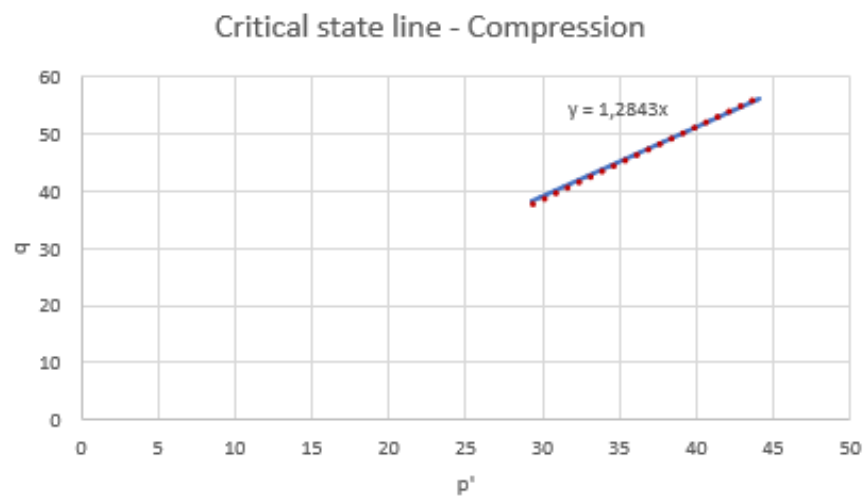
Figure A.5: The critical state line of the static data in compression.

A.2 CAUE

Figure A.6: A graph showing the axial strain, ε_a, to q for static sample 8.
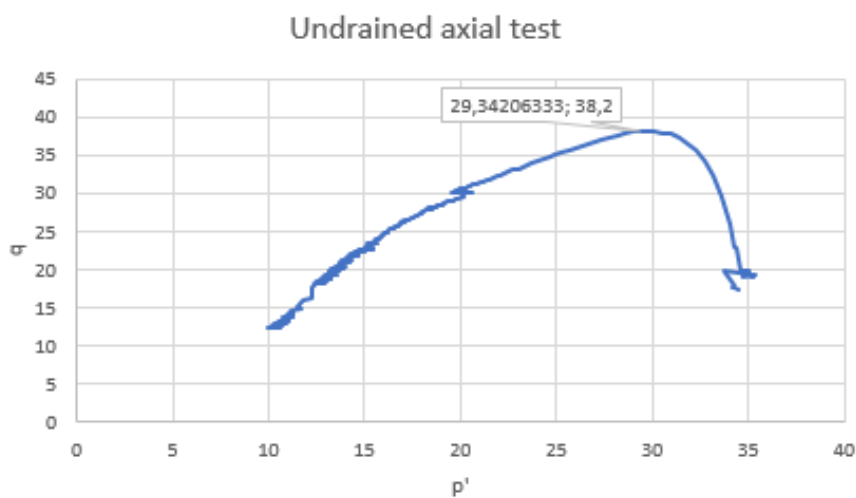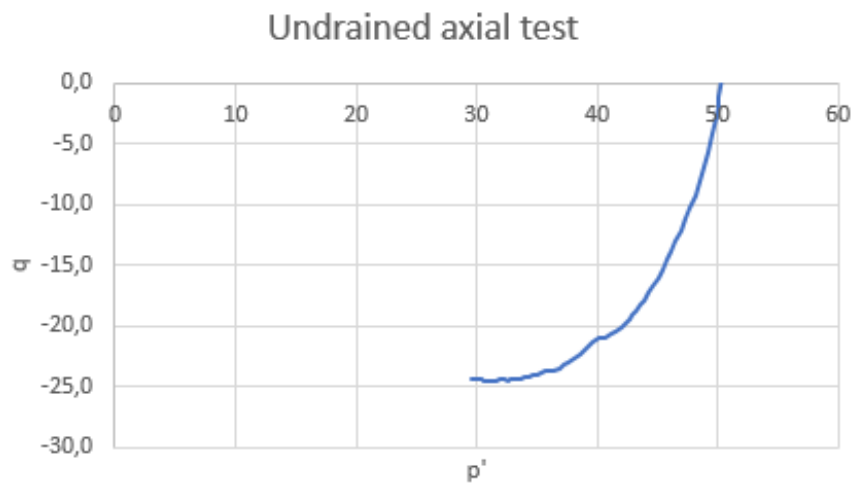

Figure A.7: A graph showing p to q for static sample 8.
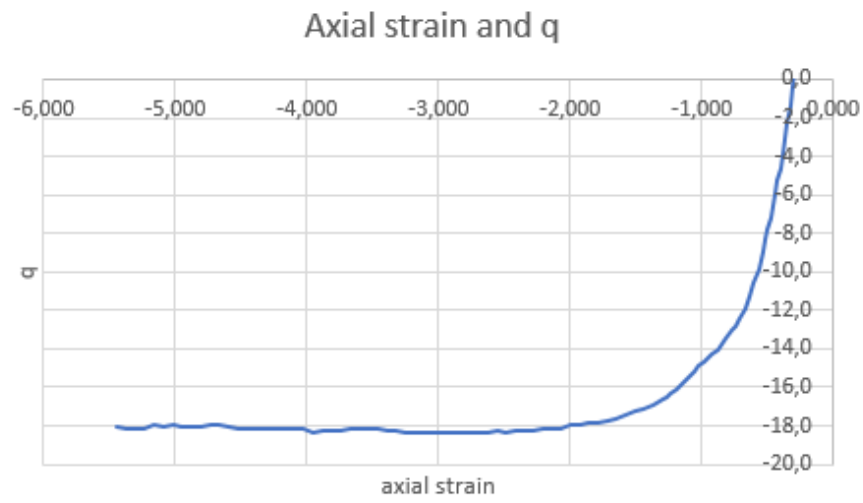
Figure A.8: A graph showing the axial strain, ε_a, to q for static sample 32.

Figure A.9: A graph showing p to q for static sample 32.
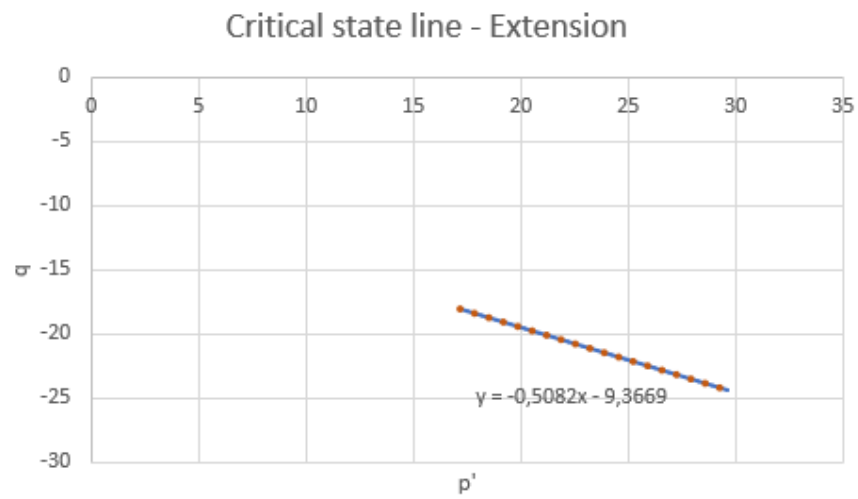
Figure A.10: The critical state line of the static data in extension.
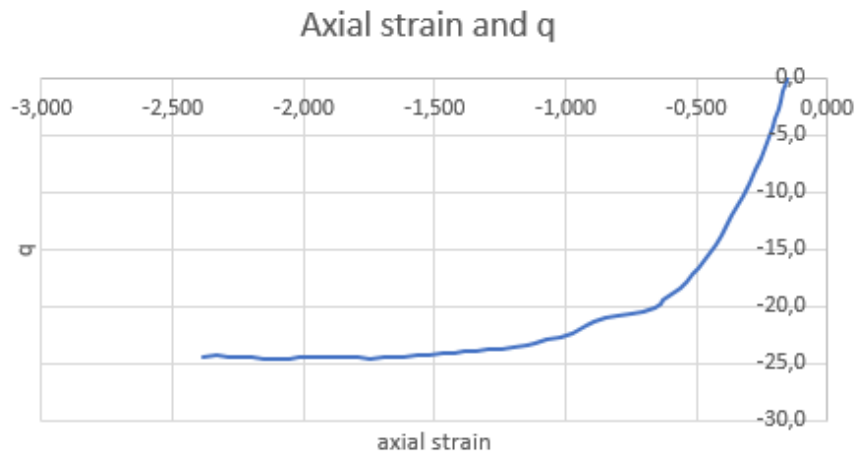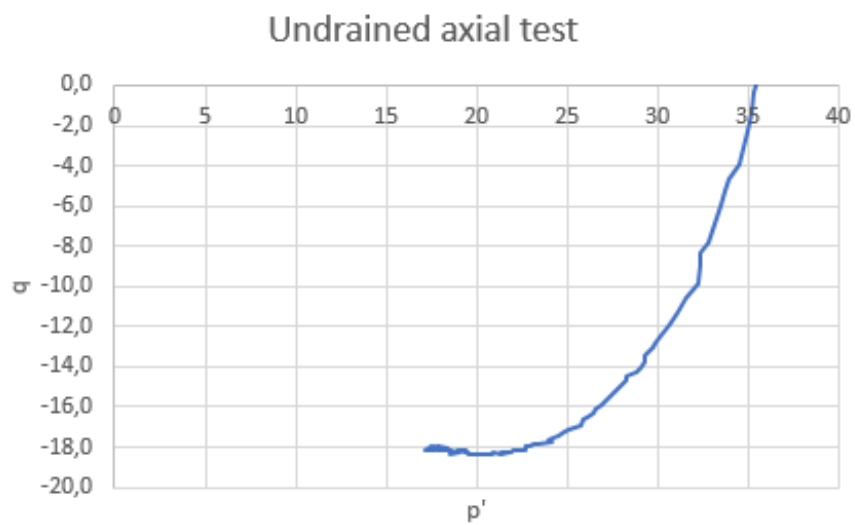
B
Appendix B

Parameters

Table B.1: General parameters.

General Parameters	Unit	Value
Gravity, g	[m/s^2]	9.82
Wave amplitude	[m]	15
Wave frequency	[Hz]	0.10
Water depth	[m]	50

Table B.2: Load parameters (Byrne, 2011).

Load Parameters	Unit	Min Value	Max Value
F$_{wind}$	[MN]	1	2
F$_{wave}$	[MN]	3	8
M$_{wind}$	[MNm]	158	342
M$_{wave}$	[MNm]	150	400
F$_{h,tot}$	[MN]	4	10
M$_{tot}$	[MNm]	308	742

Table B.3: Wind turbine parameters.

Wind turbine parameters	Unit	Value
h$_{hub}$	[m]	90
h$_{turbine}$	[m]	153
m$_{rotor}$	[kg]	110 000
m$_{nacelle}$	[kg]	240 000
m$_{tower}$	[kg]	347 460
m$_{tot}$	[kg]	697 460
F$_v$	[MN]	6.85

Table B.4: Jacket parameters (4C Offshore, 2018).

Jacket parameters	Unit	Min Value	Max Value
h$_{jacket}$	[m]	68	81
m$_{jacket}$	[kg]	1 000 000	1 150 000
F$_v$	[MN]	9.82	11.29

Table B.5: Foundation parameters.

Foundation Parameters	Unit	Min Value	Max Value
F_v	[MN]	16.67	18.14
F_h	[MN]	4.00	10.0
F_{v_i}	[MN]	4.17	4.54
F_{h_i}	[MN]	1.00	2.50
$\mathrm{Area}_{suction\ caisson\ lid}$	[m^2]	50.0	50.0
σ_{v_i}	[kPa]	82.91	90.23
σ_{h_i}	[kPa]	20.00	50.00

C
Appendix C

PLAXIS 2D
Element Properties

Table C.1: Properties of plate element (Plaxis, 2018).

Parameter		Value
Material type	[-]	Elastic; Isotropic
EA	[kN/m]	7.5×10^6
EI	[kNm^2/m]	1.0×10^6
w	[kN/m/m]	10.0
v	[-]	0.0

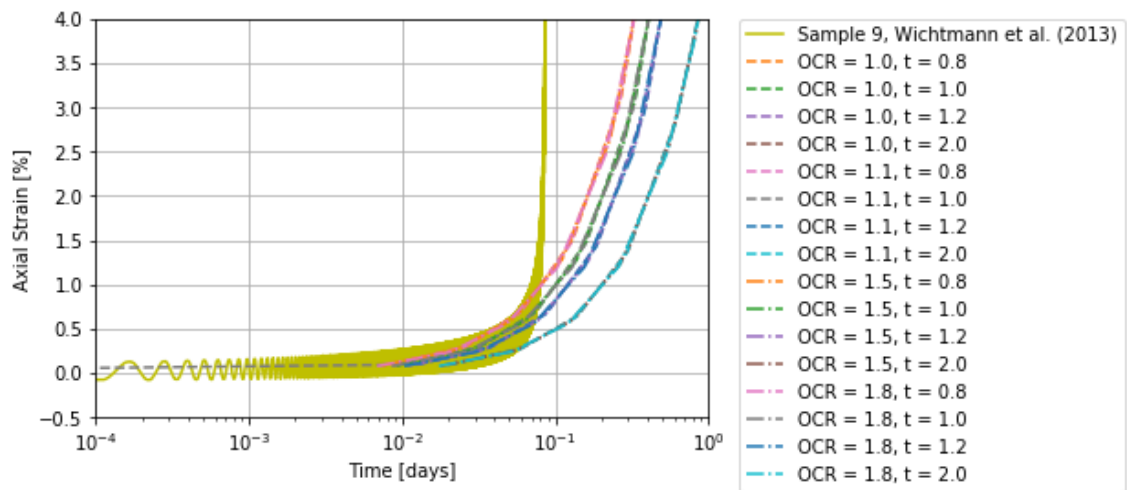# D
Appendix D

OCR Dependence

Figure D.1: Graphical representation of table D.1 and D.2.

Table D.1: Axial strain to time, triaxial soil test output for different OCR and time-periods.

	OCR 1	OCR 1.1
	Time [day] ε_1 [%]	Time [day] ε_1 [%]
0.8 days	0 0	0 0
	12.5637860265297 0.100986299153755	12.1226982639447 0.097440736992807
	37.691358079589 0.302936068792773	36.3680947918341 0.292296431380968
	87.9465021857075 0.706766762006531	84.8588878476128 0.681940841958442
	188.456790397945 1.51436729227443	181.840473959171 1.46116973382495
	389.477366822419 3.12949656581358	375.803646182286 3.01955683324997
	791.518519671369 6.35965685482923	763.729990628515 6.13623497979396
	1152 9.25585538045292	1151.65633507475 9.25286010654735
1.0 days	Time [day] ε_1 [%]	Time [day] ε_1 [%]
	0 0	0 0
	15.4627554676035 0.0994301249095629	14.9474913298668 0.0961166445774242
	46.3882664028106 0.298268312079193	44.8424739896003 0.288324855281435
	108.239288273225 0.695875435346948	104.632439309067 0.672673907564392
	231.941332014052 1.4910272740305	224.212369948001 1.44131061679532
	479.345419495709 3.081254836167	463.37223122587 2.97850919013752
	974.153594459022 6.26159934988289	941.691953781606 6.05279842902605
	1440 9.25572535721745	1440 9.25542272473858
1.2 days	Time [day] ε_1 [%]	Time [day] ε_1 [%]
	0 0	0 0
	18.2817180391568 0.0979638988823034	17.7037180236667 0.0948664379071716
	54.8451541174702 0.293870257218363	53.1111540709999 0.284574822252783
	127.972026274097 0.685613475117647	123.926026165666 0.663923975619944
	274.225770587351 1.46903595015142	265.555770354999 1.42255941162368
	566.733259213858 3.03580032467271	548.815258733665 2.93975113433368
	1151.74823646687 6.16920517808505	1115.334235491 5.97401390925439
	1439.87411823344 7.71235576684454	1398.59372386966 7.491065703822
	1583.93705911672 8.48252574159128	1540.22346805899 8.24896852081402
	1655.96852955836 8.86677391478559	1681.85321224832 9.00436311079201
	1728 9.24973537834967	1728 9.24989535094307
2.0 days	Time [day] ε_1 [%]	Time [day] ε_1 [%]
	0 0	0 0
	28.8808344256722 0.0928553653122941	28.1454420048912 0.0904906879216285
	86.6425032770167 0.278546353363974	84.4363260146737 0.271449220839168
	202.165840979706 0.649858613464579	197.018094034238 0.633298375654034
	433.212516385083 1.39241286762851	422.181630073368 1.35692775272313
	895.305867195839 2.87742162878715	872.508702151629 2.80408870971231
	1357.39921800659 4.36176472599792	1322.83577422989 4.25060297680646
	1588.44589341198 5.1034476391138	1547.99931026902 4.97376159850823
	1703.96923111466 5.47352547674252	1660.58107828858 5.33488127503881
	1935.01590652004 6.20498465698924	1885.74461432771 6.05071712442696
	2050.53924422272 6.56512061263523	1998.32638234728 6.40497095408564
	2166.06258192541 6.916840965688	2110.90815036684 6.75233763474907
	2281.58591962811 7.2527209056685	2223.4899183864 7.08983069280809
	2397.1092573308 7.56830942649148	2336.07168640597 7.40954547761778
	2512.63259503348 7.85750934544487	2448.65345442553 7.70749229133169
	2628.15593273617 8.1127335646506	2561.2352224451 7.97827583579158
	2743.67927043886 8.32827748455851	2673.81699046466 8.21268571356446
	2859.20260814156 8.51349828230048	2786.39875848423 8.41509045400287
	2880 8.54670979807659	2880 8.57845159247334

Table D.2: Axial strain to time, triaxial soil test output for different OCR and time-periods.

|	OCR 1.5	OCR 1.8
0.8 days	**Time [day] ε_1 [%]**	**Time [day] ε_1 [%]**
	0 0	0 0
	10.6591841518055 0.0856757023770605	9.89737356889767 0.0795462633715679
	31.9775524554167 0.256980248598594	29.692120706693 0.238574022367678
	74.6142890626388 0.599532164411436	69.2816149822837 0.556581406411161
	159.887762277083 1.28458032167403	148.460603533465 1.19254403538825
	330.434708705971 2.6546105889944	306.818580635827 2.46440718533375
	671.52860156375 5.39458328547155	623.534534840553 5.00805150100123
	1152 9.25404803221899	1152 9.25220535362723
1.0 days	**Time [day] ε_1 [%]**	**Time [day] ε_1 [%]**
	0 0	0 0
	13.2385294968205 0.0851257556720436	14.9474913298668 0.0961166445774242
	39.7155884904614 0.255331699297813	44.8424739896003 0.288324855281435
	92.6697064777432 0.595686221746526	104.632439309067 0.672673907564392
	198.577942452307 1.27633846790294	224.212369948001 1.44131061679532
	410.394414401434 2.63757324279283	463.37223122587 2.97850919013752
	834.027358299687 5.35994451717642	941.691953781606 6.05279842902605
	1440 9.25386479135695	1440 9.25542272473858
1.2 days	**Time [day] ε_1 [%]**	**Time [day] ε_1 [%]**
	0 0	0 0
	15.7895632127736 0.0846072874760447	14.8870723402909 0.079764032417517
	47.3686896383209 0.253777426268975	44.6612170208728 0.23923199974817
	110.526942489416 0.59206019552874	104.209506382037 0.558119086532664
	236.843448191605 1.26856775388131	223.306085104364 1.19583880825698
	489.476459595983 2.62150929891432	461.49924254902 2.47120853169465
	994.742482404741 5.32728283645489	937.88555743833 5.021844649484
	1500.0085052135 8.03189374632192	1332.94277871917 7.13635407316884
	1614.00425260674 8.64080871914439	1530.47138935958 8.1935106964243
	1728 9.24679105632552	1629.2356946798 8.7211444666327
		1728 9.24695955052511
2.0 days	**Time [day] ε_1 [%]**	**Time [day] ε_1 [%]**
	0 0	0 0
	25.755162560895 0.0828027684435804	24.9996717959131 0.0803651999089284
	77.2654876826851 0.248367158365798	74.9990153877392 0.24104143534553
	180.286137926266 0.579438068070262	174.997702571391 0.562344259278838
	386.327438413425 1.24151667323279	374.995076938695 1.20489010148534
	798.410039387746 2.56558305221487	774.989825673305 2.48989416444231
	1210.49264036207 3.88906117225068	1174.98457440791 3.77432681645016
	1622.57524133639 5.21131681833247	1574.97932314253 5.05771258886968
	1828.61654182354 5.86855027022796	1774.97669750983 5.69706300443494
	1931.63719206712 6.19492310959311	1874.97538469348 6.01496531630697
	2034.65784231071 6.51682076754516	2074.97275906078 6.63652906297936
	2137.67849255429 6.83213561813188	2174.97144624444 6.94006403106782
	2240.69914279787 7.13861394593499	2274.97013342808 7.23397442969375
	2343.71979304144 7.42902833461098	2374.96882061174 7.51343201550194
	2446.74044328502 7.70027716242007	2474.96750779539 7.77308921873078
	2549.7610935286 7.94769636518753	2574.96619497905 8.0084457862386
	2652.78174377219 8.16825762211077	2674.96488216269 8.21712666401985
	2755.80239401577 8.36178425143377	2774.96356934635 8.39947319438544
	2858.82304425935 8.53076349349547	2874.96225653 8.56916528120462
	2880 8.56527150763847	2880 8.57817783197835

E

Appendix E

PLAXIS 2D
Results
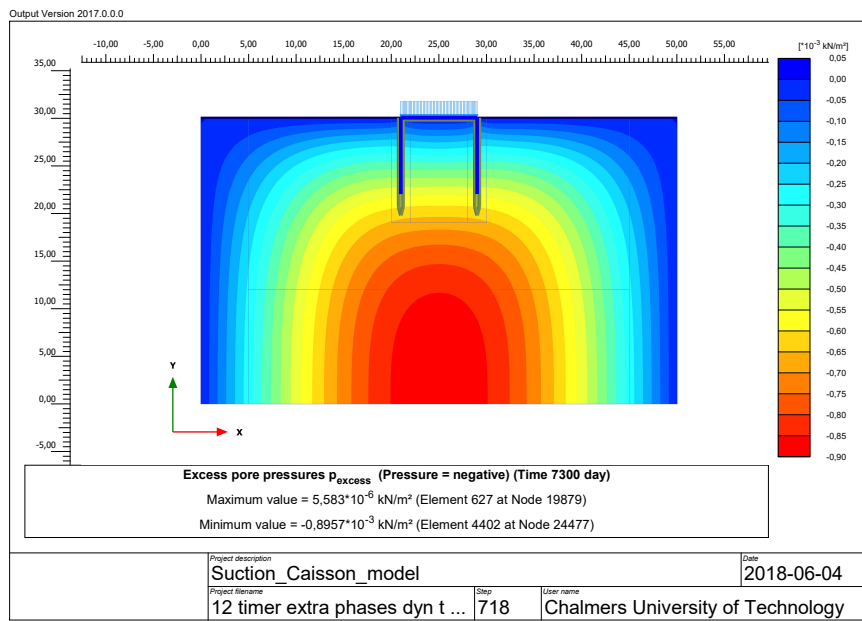
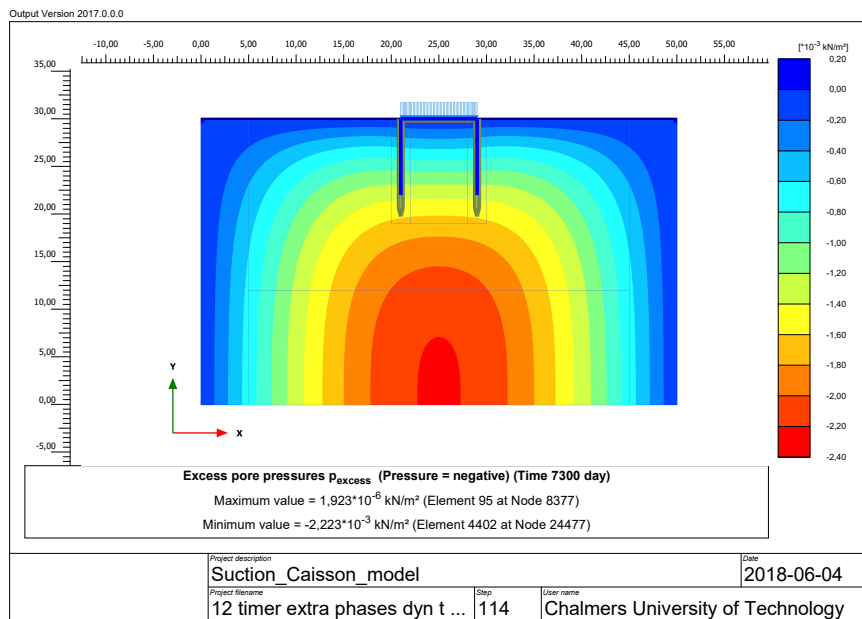**Figure E.1:** Excess Pore pressure under consolidation, SSC model

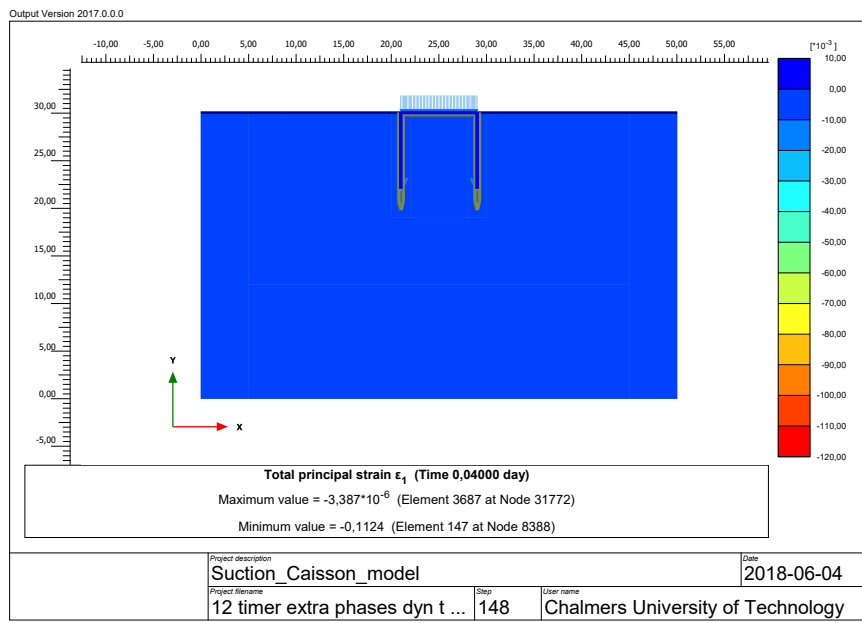**Figure E.2:** Excess Pore pressure under consolidation, SS model
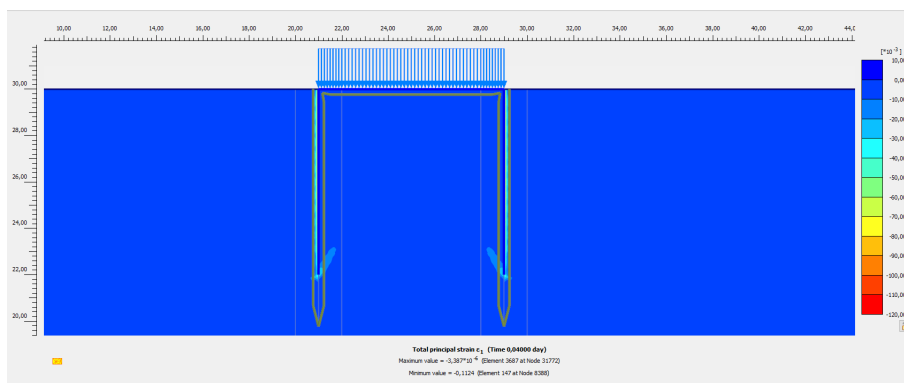
Figure E.3: Total Principle Strain, SSC
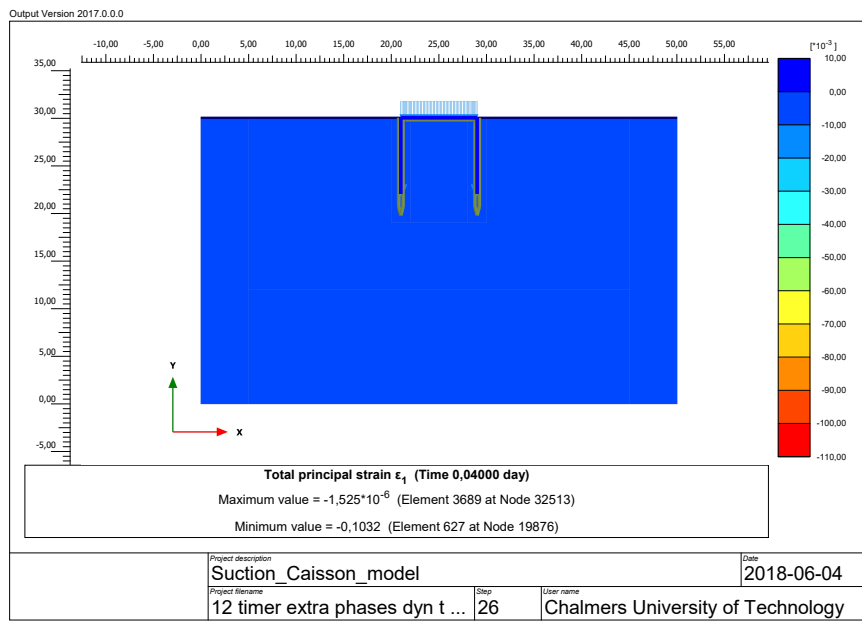

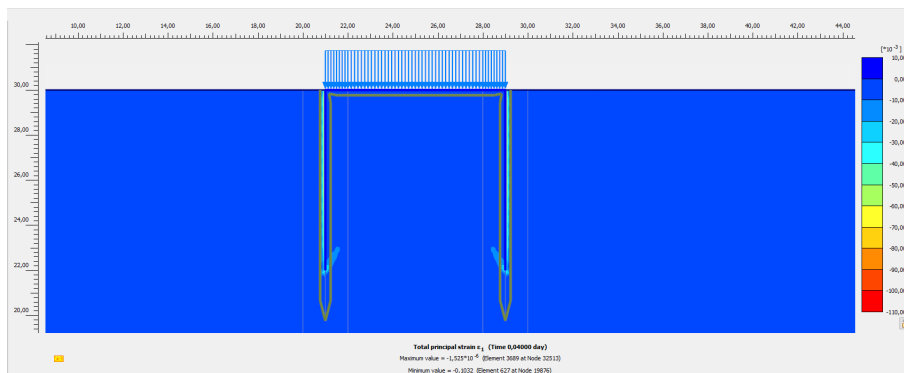**Figure E.4:** Detailed Total Principle Strain, SSC

Figure E.5: Total Principle Strain, SS

Figure E.6: Detailed Total Principle Strain, SS